THE PENNSYLVANIA STATE UNIVERSITY
SCHREYER HONORS COLLEGE

DEPARTMENT OF MECHANICAL ENGINEERING

# Novel Computer Modeling Approach for Total Knee Replacements

ANTHONY MANNARINO IV
SPRING 2022

A thesis
submitted in partial fulfillment
of the requirements
for baccalaureate degrees
in Mechanical Engineering and Spanish
with honors in Mechanical Engineering

Reviewed and approved* by the following:

Dr. Stephen Piazza
Professor of Kinesiology
Thesis Supervisor

Dr. Daniel Humberto Cortes Correales
Assistant Professor of Mechanical Engineering
Honors Adviser

* Electronic approvals are on file.

**ABSTRACT**

Computational models are effective tools in widespread use for studying knee mechanics. However, there is currently a need for fast and computationally efficient methods for rapidly evaluating how changes to the geometry of natural and artificial knees affect joint and muscle function. This thesis presents three planar equilibrium models of the human knee. The models were based on systems of nonlinear equations, which described the static equilibrium and geometry of the knee. The first model, the Natural Knee Model, was used to study the impact of Osgood-Schlatter disease on the knee extensor mechanism. The second model, the Hinged TKR Model, was used to study design considerations in a hinged knee implant. The third model, the Hinged TKR Model with Knee Simulator Input, was used to augment the Penn State Knee Simulator and predict measurements in a real-world mechanical simulation. These three analyses uncovered structure-function relationships in natural and artificial knees, demonstrating the utility of the models. Ultimately, the planar equilibrium modeling paradigm proved to be a computationally efficient method for studying knee mechanics.

TABLE OF CONTENTS

# LIST OF FIGURES

## LIST OF TABLES

## ACKNOWLEDGEMENTS

First and foremost, I dedicate this thesis to God. In the words of 2 Timothy 4:7, "*I have fought the good fight, I have finished the race, I have kept the faith.",* all because of His perfect love. Second, I dedicate this thesis to my family. To Mom, Dad, Jack, and Meg— your unconditional love and support has lifted me up on so many days when I felt anxious, discouraged, and alone. Thank you for being my biggest supporters and for your steadfast belief in me. To my grandparents, Anthony and Louise Mannarino, Thomas and Florence Fagan, for making education a priority in our family. Third, I dedicate this thesis to my friends. Ben, Erin, Josiah, Arianna, Kevin, Shagun, Steve, Johnny, the Junkyard boys, and countless others— thank you for loving me for who I am and shaping me into the person I am today.

To Dr. Piazza, I can't thank you enough for investing so much time and energy in me for the past two and a half years. I have learned more from you than any other professor, and I will carry my experience in the Biomechanics Lab with me forever. To THON, Blue Band, and Alliance Christian Fellowship, thank you for making Penn State my home for four years.

Por último, pero no menos importante, querido Manolo— muchas gracias por apoyarme en todo. Te quiero muchísimo, caballero.

# Chapter 1

# Introduction

In 2010, an estimated 693,400 total knee arthroplasty (TKA) surgeries were performed in the United States, a figure that almost doubled from 2000 [1]. TKA is a common procedure employed when the knee joint is severely damaged and cannot be repaired using alternative surgeries or therapies. More than 95% of TKAs are done to treat osteoarthritis, a disease that leads to severe bone degradation within joints [2]. Before undergoing a TKA, patients tend to report consistent pain and difficulty performing everyday activities, such using stairs and rising from a chair. The number of TKA procedures in the United States is expected to increase to 1.27 million in 2025, 1.92 million in 2030, and 3.42 million in 2040 [3]. As a result, there is increased demand for more effective and longer lasting knee replacement implants. For those who suffer from osteoarthritis, TKA is a procedure that promises to significantly reduce pain and allow a comfortable return to everyday activity. Innovation in TKA requires balancing the needs of surgeons and their patients against manufacturing and economic considerations. In addition, pre- and post-operative factors play an important role in TKA outcomes [2]. As the industry continues to expand, medical device companies are developing new implants and surgical procedures that they believe will produce the best patient outcomes possible.

Computer modeling is an essential step in the design process of knee replacement implants because it allows for the rapid evaluation of potential designs without having to build physical prototypes. The most common approach to computational knee models is the finite element method (FEM) [4]. This method begins with a continuous 3D model of the knee, then divides it into discrete elements, then solves differential stress and strain equations at each element. FEM models are powerful tools that can reveal the biomechanics of the knee on the cell, tissue, and joint levels. Modern FEM models accurately simulate the material properties of knee components like bone, ligaments, and the meniscus, making them valuable but also computationally expensive. Dynamic, time-dependent simulations that involve knee motion are particularly expensive because stress and strain equations must be solved at each time step. The limitations of FEM models arise from this computational complexity and that their solutions represent approximations according to set tolerances.

Another type of knee model employs a system of equations that describes the dynamics of the knee joint. Unlike FEM models, which are based on constitutive relations and geometric compatibility at the level of small elements, these dynamic (or “static” if no accelerations are present) mathematical models solve equations that describe the motions and interactions of whole bodies. Such models are commonly used in biomechanics research. Often we seek to make measurements that would be impossible in human subjects and impractical in mechanical models, such as the exact location of a contact point, tension within a ligament, or contact force deep within a joint. In addition to making difficult measurements, computer models allow us to perform analyses that would otherwise be impossible in human subjects, such as a sensitivity analysis that studies how changes in the geometry of the knee affect its function.

While static and dynamic knee models are commonly used in biomechanics research, current models do not fully address the needs of implant engineers. Existing models allow for a better understanding of the dynamics of the knee joint, but they are seldom used to evaluate potential knee replacements designs and compare the impact of certain design criteria against others. Therefore, there is need for a mathematical knee model that can rapidly evaluate potential implant designs.

The purpose of this thesis is to expand upon the current research by developing a two-dimensional modeling paradigm of the human knee. For this study, three distinct mathematical models will be developed, and sensitivity analyses will be performed to evaluate the impact of various design criteria on the performance of hinged knee replacement implants. The three models are described as follows:

1. **"Natural Knee Model" –** The Natural Knee Model is a two-dimensional mathematical simulation that models the natural human knee in the sagittal plane. The model is described by nine equations originally derived by Yamaguchi and Zajac [5]. These equations describe the static equilibrium and geometric compatibility of the tibia, femur, and patella. After the initial verification of the model, a sensitivity analysis will be performed that explores the impact of Osgood-Schlatter (OS) on the knee joint extensor mechanism. OS is a common disease characterized by the lengthening of the tibial tubercle. This analysis will help evaluate the robustness of the model and determine its ability to simulate the impacts of structural changes in the knee.
2. **"Hinged TKR Model" –** The Hinged TKR Model is a two-dimensional mathematical model that simulates a commercially available hinged knee replacement in the sagittal plane. The model is described by seven equations that describe the static equilibrium and geometric compatibility of the tibia, femur, and patella. A generalized approach to knee geometry is used that models contact surfaces as splines that can be adjusted to model various implant geometries. After

the initial verification of the model, a sensitivity analysis will be performed that explores the impact of the anterior-posterior position of the hinge.

3. **"Hinged TKR Model with Knee Simulator Input" –** The Hinged TKR Model with Knee Simulator Input will augment the second model by including data collected by the Penn State Knee Simulator (PSKS). The data collected from this benchtop testing will then be fed into the mathematical model to make it more realistic. The output of the subsequent simulation trials will be compared against the output of the PSKS to determine the correspondence between the computer model and benchtop testing rig.

# Chapter 2

# Literature Review

## 2.1 Overview of Total Knee Replacement

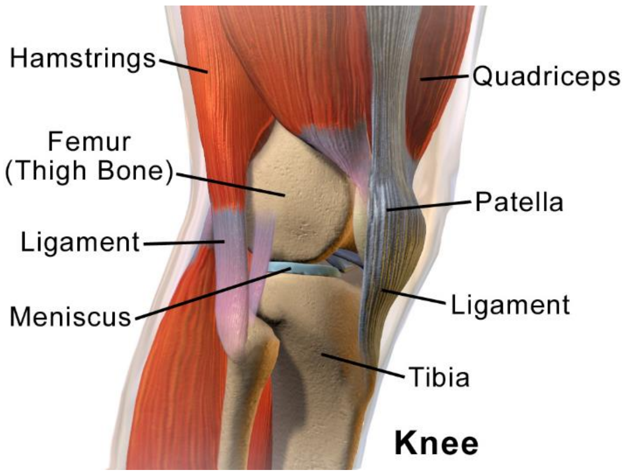


**Figure 1.** Anatomy of the human knee.
"File:Blausen 0597 KneeAnatomy Side.png" by BruceBlaus is licensed with CC BY 3.0.

We begin our discussion with a review of basic knee anatomy. As seen in Figure 1, The knee joint is made of the femur, tibia, and patella, which are held together by tendons and ligaments[6]. The femur extends from the hip to the knee, while the tibia extends from the knee to the ankle. The patella sits on top of the tibia and is held in place by the patellar tendon and the patellar ligament. The patellar tendon, also called the quadriceps tendon, links the quadriceps to the patella, and the patellar ligament links the patella to the tibia. The knee joint is constrained and stabilized by four main ligaments: the posterior cruciate ligament (PCL), anterior cruciate ligament (ACL), lateral collateral ligament (LCL), and medial collateral ligament (MCL). The PCL is of particular interest in TKR because some implant designs retain the PCL while others remove it [7]. Between the femur and tibia lies the medial and lateral menisci, which act like cushions, preventing the tibia and femur from contacting each other. When the menisci begin to deteriorate, friction develops between the femur and tibia, leading to the bone degradation disease osteoarthritis, which is the root cause of 95% of TKR surgeries [2].

The first TKRs were developed during the 1960's and featured relatively simple designs. They were hinged prostheses that allowed motion about a single axis, typically made of stainless steel. These implants were revolutionary for their time but often succumbed to infection and mechanical failure in the long term [8]. Nevertheless, as the orthopedic industry realized the potential of TKR surgery, knee replacements became more common, and their designs evolved dramatically.

In his 2012 journal article "The history of total knee arthroplasty" [9], Ranawat recounts the breakthroughs that lead to modern TKR implants. In the early 1970's, condylar designs were developed that more closely mimicked the natural anatomy of the knee. These designs offered far more range of motion than the earlier hinged implants and vastly improved patient outcomes. As novel iterations of the condylar design emerged during the 1980's, 1990's, and 2000's, certain design criteria became ubiquitous such as deformity correction, modularity, and surgical instrumentation. More recently, advances in material science and design methodology have produced high-performance, long-lasting implants. The development of titanium and cobalt-chromium alloys have led to femoral components that accelerate the healing process and increase wear resistance [10], while the use of functionally graded materials in the tibial tray has reduced the strain on implant components [11].

Currently, TKR implants can be divided into two main categories- hinged and non-hinged. As the name suggests, hinged implants feature a hinge that connects the femur and tibia. Some additional mobility is built into the hinge, allowing for more natural movement that was greatly lacking in early hinged designs [12], [13]. Hinged implants are primarily used in elderly and revision cases where significant stability is desired, and some natural knee motion must be constrained. On the other hand, non-hinged TKR implants are more common and offer a greater range of motion [9], [14]. Some designs retain the cruciate ligaments, while others elect to remove them and mechanically stabilize the implant. Both categories of implants tend to reduce pain and increase quality of life, but non-hinged condylar implants often allow patients to resume normal activity with significantly reduced pain, making them the more popular of the two categories. This study will focus on how hinged implants can be improved to produce excellent outcomes in elderly and revision cases.

Post-operative patient satisfaction is how implant manufacturers and designers measure success. In 2018, a team of researchers conducted a comprehensive review of patient satisfaction after TKR, synthesizing the outcomes of over 90,000 patients [15]. The team found that post-operative satisfaction levels ranged from 80 to 100%, and studies that featured a 0-10 satisfaction scale reported means above 7.0. The best predictors of patient satisfaction were reduction of pain and improved range of motion, while the best predictors of dissatisfaction were preoperative anxiety, persistent pain, and requiring revision surgery. This study highlighted how far knee arthroplasty had come since its inception and highlighted the areas where the procedure could continue to improve.

Another goal of modern knee replacement is to improve implant longevity. As osteoarthritis incidence increases, more patients look to knee replacements to mitigate their pain. As a result, rates of TKR continue to increase and demographics are shifting younger. Implant engineers now face the challenge of creating implants that can last up to 30 years and beyond [16]. Currently, 82% of TKRs last 25 years, meaning patients who receive them in their late 50's and early 60's risk implant failure during the latter years of their life [17]. Sustained advancements in implant design and surgical techniques are necessary to continue the success of TKRs and reduce revision surgery rates as demographics shift.

## 2.2 Technical Design Considerations in TKR

As engineers and surgeons work together to improve current implants and surgical procedures, they must balance a variety of design criteria. The modern TKR implant has a complex construction that can be modified in a variety of ways, while modern surgical techniques allow for excellent precision when positioning and installing the implant. The design considerations most relevant to our discussion of hinged implants are the location of the position of the hinge, location of the joint line, and position of the patella. These three criteria must be intricately balanced during implant design and surgery to produce the best patient outcomes.

The most pertinent design consideration for hinged implants is the location and construction of the hinge itself. In particular, the anterior-posterior position of the hinge greatly influences implant functionality [18]. It is assumed that a more posterior hinge increases the moment arm, and hence the leverage, of the quadriceps, but this phenomenon is not well documented. Furthermore, a more posterior hinge can reduce the need for bone resection but may also cause abnormal patella motion [18]. Today, modern hinged implants allow for slight rotation about the long axis of the tibia, and this added degree of freedom allows for more natural knee motion. However, the degree to which this freedom impacts implant performance is not well understood. The position and construction of the hinge impacts implant performance, but this impact has not been thoroughly explored in the existing literature.

Another relevant design criterion is the location of the joint line, which refers to the proximal-distal position of the axis of rotation of the knee. When performing knee arthroplasty, surgeons can alter the position of the joint-line through resection of the tibia and femur surfaces. Particularly during revision surgery, significant portions of the femur and tibia must be resected to allow healthy bone surfaces to accommodate the implant. Regarding surgical procedures, multiple researchers [19], [20] suggest the joint line should be maintained at its natural position to avoid increased patellofemoral contact forces, which can lead to pain and degradation of the implant. However, bone deformity due to osteoarthritis and implant wear also plays a role in determining tibia and femur resection, which in turn affects joint line position. In summary, the issue of where to place the joint line during revision surgery remains unresolved, and further investigation is necessary to determine which surgical approach produces the best results in the long-term.

The location of the joint line is intimately linked to the position of the patella— a more proximal joint line leads to a more distal patella, and vice versa [21]. An abnormally proximal patella is called patella alta, while an abnormally distal patella is called patella baja. Patella alta and baja are often studied outside the context of knee arthroplasty because of their impact on knee mechanics [22]. Specifically, patella alta is associated with increased quadriceps moment arm, while patella baja tends to decrease moment arm but to a lesser extent [23]. The location of the joint line, along with the lengthening or shortening of the patellar ligament, can influence knee mechanics by altering the position of the patella. Surgeons must take great care to balance the positions of the femur, tibia, and patella, which can be accomplished using appropriately designed instruments [24]. In addition, a more thorough understanding of structure-function relationships in the knee will help surgeons make these decisions with greater confidence and produce consistently positive outcomes.

## 2.3 Overview of Mathematical Knee Models

Mathematical models are a powerful tool commonly used in biomechanics research. Mathematical models simulate the biomechanics of human motion by studying components of the body as mechanical systems. Equations are developed to describe the system according to given criteria, assumptions, and limitations. Depending on the nature of the system of equations it may be solved explicitly or numerically. In the case of the knee, 3D mathematical models often produce an underdefined system of equations, making them difficult to solve. In 1980, Wismans et al. remedied this by modelling only the tibia-femoral joint and assuming no deformation at the contact point [25]. Despite these simplifications, their work proved revolutionary and became the foundation of countless future models. Later on, mathematical models were developed that simulated tibia-femoral deformation [26] and patella-femoral dynamics [27].

Yamaguchi and Zajac pioneered the framework for 2D mathematical knee models in their 1989 paper “A Planar Model of the Knee Joint to Characterize the Knee Joint Extensor Mechanism” [5], which featured a sagittal-plane model based on static equilibrium and the geometric compatibility of the femur, tibia, and patella. The two authors used measurements made in human subjects to formulate their equations and make them as accurate as possible. In particular, the Yamaguchi and Zajac model prescribed the location of the tibiofemoral contact point at every angle of knee flexion. This ensured that the motion of the 2D model would reflect the actual 3D motion of the knee in the sagittal plane. By using 3D measurements to inform their

2D model, Yamaguchi and Zajac created a powerful, efficient tool that characterized structure-function relationships in the knee. This study will build on their work by applying their methodology to knee replacement implants and using a mechanical knee simulator to augment the mathematical model.

The utility of computer models depends on our ability to verify and validate them [28], [29]. Verification ensures that the algorithms and code used to solve the model are implemented correctly. Before any data or insight can be gleaned from a model, researchers much confirm that it functions exactly as intended; otherwise, the results will not be meaningful. Once a model is verified, it can offer significant insight into the biomechanics of a system; however, the model must be validated to determine if these insights are representative of actual phenomena that occur *in vivo*. Models are validated by comparing their results to independent datasets and to previously validated models, which ensures they are an accurate representation of actual biomechanical systems. Currently, knee models cannot be completely validated because *in vivo* measurements are exceptionally difficult to make; however, rigorous verification allows knee models to still be valuable [4]. This study will seek to validate a computer model of the knee by comparing it to outputs obtained using a physical knee simulator.

## 2.4 Overview of Oxford Rig-Style Knee Simulators

A knee simulator is an *in vitro* testing apparatus used to study the human knee and test knee implants. There are two main types— Oxford simulators and robotic simulators, both of which may use artificial knee components or cadaver specimens [30]. Oxford simulators originate from the work of Zavatsky [31] and generally have 6 degrees of freedom. They simulate a squatting motion by exerting a quadriceps force on the system and collect data by measuring loads and tracking segment positions. On the other hand, robotic simulators simulate knee flexion by securing the tibia in place and applying a varying force to the femur along a prescribed path. The force applied by the robot has six degrees of freedom and as a result is more customizable than the Oxford rig. While both paradigms have their limitations, they have proved valuable to our understanding of knee kinematics [30].

Since the original work of Zavatsky [31], many researchers have developed more advanced Oxford rig simulators. Long et al. [32] used an Oxford rig to study structure-function relationships in hinged knee replacements. After measuring the quadriceps and patellar tendon moment arm in five commercially available implants, they determined the design criteria that most affect quadriceps force. In addition, Maletsky et al. used the Purdue Knee Simulator in conjunction with a mathematical model to explore the dynamics of the knee [33]. Their Oxford rig simulator measured tibiofemoral compressive force and quadriceps tension, but they did not use this methodology to study knee implants.

Although they are a powerful tool for biomechanics research, Oxford rig simulators have limitations. One limitation is that the data collected relies heavily on the prescribed force applied by the quadriceps actuator, as the magnitude of this loading can significantly affect knee kinematics [30]. Another limitation of Oxford rig simulators is the difficulty of collecting data. Quadriceps force, patellofemoral contact force, and kinematic data are frequently measured, but data such as the tibiofemoral contact force, contact point location, and reaction force of the hinge are all useful metrics remain impossible to measure using current approaches. This thesis will seek to address these limitations by using the Penn State Knee Simulator in conjunction with a mathematical model to evaluate a hinged knee implant. We suspect that using the two in concert will provide a more nuanced and well-rounded understanding of knee implant dynamics.

# Chapter 3

# Methods

Three mathematical knee models were developed and used to study structure-function relationships in the knee joint extensor mechanism. The three models were termed the "Natural Knee Model", the "Hinged TKR Model", and the "Hinged TKR Model with Knee Simulator Input". All three models were developed in MATLAB and featured input parameters, a system of equations that was solved numerically, and postprocessing that analyzed each model's output. Each model had distinct features and was used to study specific aspects of the knee. The first model focused on structure-function relationships in the natural knee, the second focused on structure-function relationships in a hinged knee replacement, and the third focused on using the Penn State Knee Simulator to augment the previous model's output.

The three models were based in the Cartesian coordinate system and located in the sagittal plane. Each model had a global coordinate system whose origin was defined at the tibia, which was assumed to be fixed. Each model also had a local coordinate system defined at the femur, which rotated with the femur. This local coordinate system was created to simplify calculations and avoid computational errors during the simulation. A transformation matrix was developed in each model that transformed vectors from the femoral coordinate system to the global tibial coordinate system, and all calculations were performed with respect to the global coordinate system.

## 3.1 Natural Knee Model

The Natural Knee Model was developed using the methodology of Yamaguchi and Zajac in their 1989 paper "A Planar Model of the Knee Joint to Characterize the Knee Extensor Mechanism" [5]. The input parameters and system of equations were obtained from their paper, and their analysis of structure-function relationships was replicated. Then, this structure-function analysis was applied to study Osgood-Schlatter disease (OS). OS occurs in 10% of adolescents and causes a bump to form where the patellar ligament attaches to the tibia, making it a useful model for studying structure-function relationships in the knee.

The Natural Knee Model was based on a system of nine equations; three equations described the equilibrium of the patella, three equations described the patellofemoral (PF) contact point, and the equations described the tibiofemoral (TF) contact point. The system of equations was solved at each angle of knee flexion from 0 to 90 degrees, and all outputs were stored in 91-element vectors that corresponded with the knee flexion angle.

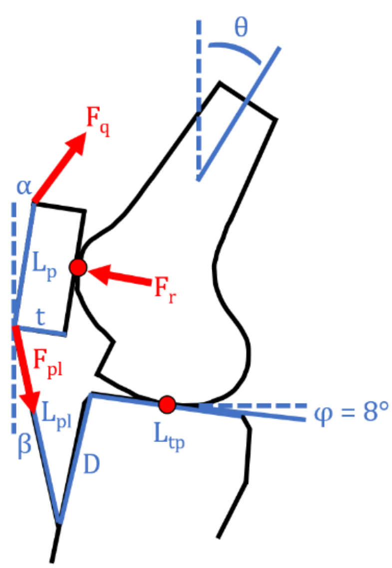


**Figure 2.** Parameters and angular definitions used in the two-dimensional model**.**

As demonstrated by Figure 2, the geometry of the knee was simplified to a two-dimensional model in the sagittal plane featuring the femur, tibia, and patella. The articulating surfaces of the femur were modeled by elliptical curves, each with two parameters describing their major and semimajor axes. Ellipse 1 modeled the femoral condyle, and Ellipse 2 modeled the median anterior groove of the femur. That is, the TF contact point occurred on Ellipse 1, and the PF contact point occurred on Ellipse 2. These ellipses were formulated as continuous curves described by the following equation:

$$\frac{x^2}{A^2} + \frac{y^2}{B^2} = 1 \qquad (1)$$

where A and B describe the major and semimajor axes respectively. In parametric form, this equation became:

$$x = Acos(\Phi) \qquad (2a)$$

$$y = Bsin(\Phi) \qquad (2b)$$

where $\Phi$ represents the ellipse parameter. $\Phi$ can be thought of the angle $(x, y)$ makes with the positive x-axis. Mathematically, both ellipses were centered about the origin and fixed in the femoral coordinate system, rotating with the femur as a single rigid body. The center of Ellipse 1 was the origin of the femoral coordinate system, and the center of Ellipse 2 was described by point $(C_x, C_y)$ in the femoral coordinate system, where $\vec{C}$ is the vector that pointed from the center of Ellipse 1 to the center of Ellipse 2.

The tibia was modeled as a straight line sloped downward at a specified angle, and the patella was modeled as a rectangle. The PF and TF contact points were mathematically described as the tangential intersection of the femur articulating surface with the patella and tibial slope respectively. In addition, the quadriceps muscle force was modeled by a single force acting at a specified “q-angle”; this force was assumed to act along the long axis of the femur.

In order to define a system of equations that could be solved at each angle, it was necessary to prescribe the movement of the TF contact point along the tibial plateau. Following the methodology of Yamaguchi and Zajac [5], the findings of Nisell et al. [34] were applied to solve this problem. A plot was obtained that described the position of the TF contact point along the tibial plateau as a function of knee flexion angle. Specifically, the position of the TF contact point was given as a percentage, where 100% represented the anterior border of the plateau.

After obtaining this plot, it was necessary to transform the data into a form that could be interpreted by MATLAB. To extract numerical data from the plot, the GRABIT app in MATLAB was used. The GRABIT app was developed independently and accessed through the MATLAB File Exchange. First, the figure was imported into GRABIT and the axis dimensions were calibrated. Then, forty points were precisely selected along the curve and exported as a MATLAB array. Once these forty data points were obtained, a spline was interpolated between them, forming a continuous mathematical representation of the data.

The Natural Knee Model required multiple input parameters that described the geometry and dynamics of the knee joint. Distances were measured in centimeters, angles in degrees, and forces in Newtons. Certain input parameters were changed as part of sensitivity analyses, but the nominal values were described as follows:

**Table 1.** Nominal input parameters of the Natural Knee Model. These inputs describe knee geometry and mathematical parameters necessary to develop the system of equations

| *Symbol* | *Definition* | *Value* | *Notes* |
|---|---|---|---|
| $\theta$ | Flexion of the femur relative to the tibial axis. Referred to as “knee flexion angle”. | 0-90 degrees | Varied at one-degree increments. |
| $\theta_q$ | Quadriceps-force angle with respect to the tibial axis (degrees) | 0-90 degrees | We assume $\theta_q$ is equal to the flexion of the femur relative to the tibial axis. |
| $\phi$ | Slope of tibial plateau | 8 degrees | |
| $F_q$ | Quadriceps force | 250 N | |
| t | Patellar thickness | 1.63 cm | |
| $L_p$ | Patellar length | 3.94 cm | |
| $L_{pl}$ | Patellar ligament length | 6.52 cm | |
| $L_{tub}$ | Length of tibial tubercle | 0 cm | Nominal tubercle length was 0 cm. This was changed during the analysis of OS. |
| $L_{tp}$ | Length of tibial plateau | 5.57 cm | |
| $P_{tp}$ | Percentage of the tibial plateau | 0-100% | |
| D | Distance from tibial tuberosity to anterior corner of tibial plateau | 5.26 cm | |
| $A_1$, $B_1$ | Major and semimajor axis lengths of Ellipse 1 | 3.54 cm, 2.18 cm | |
| $A_2$, $B_2$ | Major and semimajor axis lengths of Ellipse 2 | 2.86 cm, 1.90 cm | |
| $C_x$, $C_y$ | Vector components of $\vec{C}$, | .25 cm, .79 cm | |

These input parameters were used to define the system of nine equations describing the Natural Knee Model. The nine equations collectively described the equilibrium of the patella, the geometry of the PF contact point, and the geometry of the TF contact point. After the nine equations were derived, they were set equal to zero so they could be solved simultaneously in

MATLAB using a minimizing function. The quantities minimized were referred to as "residuals", represented by the vector $\vec{R}$. In essence, rather than solving the system for an exact solution, the solver minimized $\vec{R}$ and outputted the answer with the least overall error.

The unknowns in the system included the angle of the patella, angle of the patellar ligament, locations of the contact points, the PF contact force, and the patellar ligament force. In total, there were nine unknown variables in the system of equations, defined as follows:

**Table 2.** The nine unknown variables of the Natural Knee Model

| *Symbol* | *Definition* |
|---|---|
| **$\alpha$** | Patellar axis angle with respect to the tibial axis |
| **$\beta$** | Patellar ligament angle with respect to the tibial axis |
| **$\Phi_1$** | Parameter of Ellipse 1 where TF contact occurs. Essentially, this is the angle swept out from the positive x-axis to the TF contact point. |
| **$\Phi_2$** | Parameter of Ellipse 2 where PF contact occurs. Essentially, this is the angle swept out from the positive x-axis to the PF contact point. |
| **h** | Distance from the bottom right corner of the patella to the PF contact point. |
| **$t_x$, $t_y$** | Location of the femoral coordinate system origin in the global (tibial) coordinate system |
| **$F_r$** | Patellofemoral contact force |
| **$F_{pl}$** | Patellar ligament force |

After defining the assumptions, input parameters, and unknowns, the system of equations describing the Natural Knee Model was developed. In the following derivations, equations describing the residual vector $\vec{R}$ will be bolded, as these were the precise equations minimized by the solver.

The first three equations were developed using the static equilibrium of the patella. That is, at any given knee flexion angle, it was assumed that the forces on the patella were balanced according to the following free body diagram:

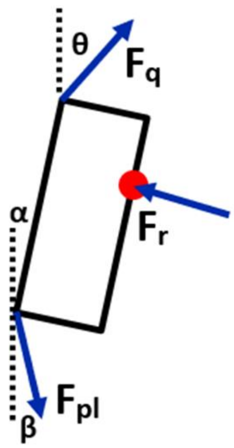


**Figure 3.** Free body diagram of the patella, with the quadriceps force, patellar ligament force, and PF contact force.

This equilibrium assumption yielded three equations, two describing static equilibrium in the x- and y- directions, and one describing the rotational static equilibrium. The first two equations were defined as follows:

$$\boldsymbol{F_r \cos\alpha + F_{pl} sin\beta - F_q sin\theta = \vec{R}(1)} \tag{3}$$

$$\boldsymbol{-F_r \sin\alpha + F_{pl} cos\beta - F_q cos\theta = \vec{R}(2)} \tag{4}$$

The third equation, describing rotational equilibrium, was derived by summing the moments due to $F_{pl}$ and $F_q$ about the PF contact point. In this case, $F_r$ was not considered in the calculation because it was applied at the contact point and did not produce a moment about that point:

$$\vec{M}_q + \vec{M}_{pl} = 0 \tag{5}$$

$$\vec{r}_q \times \vec{F}_q + \vec{r}_{pl} \times \vec{F}_{pl} = 0 \tag{6}$$

$$\begin{bmatrix} -t \\ L_p - h \\ 0 \end{bmatrix} \times \begin{bmatrix} F_q \sin(\theta - \alpha) \\ F_q \cos(\theta - \alpha) \\ 0 \end{bmatrix} + \begin{bmatrix} -t \\ -h \\ 0 \end{bmatrix} \times \begin{bmatrix} F_{pl} \sin(\alpha - \beta) \\ F_{pl} \cos(\alpha - \beta) \\ 0 \end{bmatrix} = \begin{bmatrix} \sim \\ \sim \\ \vec{R}(3) \end{bmatrix} \tag{7}$$

Where "~" was used to indicate a vector element that is not included in the residual vector. The addition of these two cross products yielded a 3 by 1 vector whose third element represented the moment in the z-direction, perpendicular to the sagittal plane, and formed the third element of the residual vector.

The next three equations described the geometric compatibility of the patella and femur at the PF contact point. In short, the equations stated that 1) The point defined on the patella had the same coordinates as the point defined on the femur and 2) The two segments could not pass through each other. These two statements were based on the assumption that the surface of the Ellipse 2 was tangent to the patella and that contact occurred at a single point. The close-up geometry of the PF contact point was as follows:

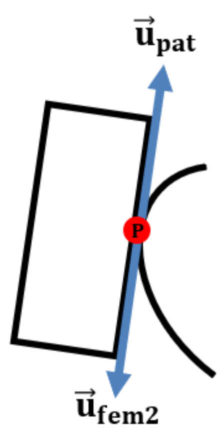


**Figure 4.** Close-up view of the PF contact point.

Where P represented the contact point, $\vec{u}_{pat}$ was the unit vector parallel to the surface of the patella, and $\vec{u}_{fem2}$ was the unit vector tangent to the surface of the femur. The agreement of the location of the contact point on the patella and femur was described as follows:

$$P_{pat}(x,y) - P_{fem2}(x,y) = 0 \tag{8}$$

Then, both $P_{pat}$ and $P_{fem2}$ were mathematically defined in the global coordinate system using a transformation matrix $T_{tf}$ that transformed points from the femur coordinate system to the global coordinate system. Because $T_{tf}$ was a four by four matrix, the points were represented using four by one vectors. The first two elements of the resulting four by one vector formed the fourth and fifth elements of the residual vector.

$$\begin{bmatrix} -\boldsymbol{L_{tub}} + \boldsymbol{L_{pl}} + \boldsymbol{tcos\alpha} + \boldsymbol{hsin\alpha} \\ \boldsymbol{L_{pl}cos\beta} - \boldsymbol{tsin\alpha} + \boldsymbol{hcos\alpha} \\ \mathbf{0} \\ \mathbf{0} \end{bmatrix} - \boldsymbol{T_{tf}} \begin{bmatrix} \boldsymbol{C_x} + \boldsymbol{A_2cos\Phi_2} \\ \boldsymbol{C_y} + \boldsymbol{B_2sin\Phi_2} \\ \mathbf{0} \\ \mathbf{0} \end{bmatrix} = \begin{bmatrix} \vec{\boldsymbol{R}}(\mathbf{4}) \\ \vec{\boldsymbol{R}}(\mathbf{5}) \\ \sim \\ \sim \end{bmatrix} \tag{9}$$

Where $T_{tf}$ was defined as follows:

$$T_{tf} = \begin{bmatrix} cos\theta & sin\theta & 0 & t_x \\ -sin\theta & cos\theta & 0 & t_y \\ 0 & 0 & 1 & 0 \\ 0 & 0 & 0 & 0 \end{bmatrix} \tag{10}$$

The final equation derived at the PF contact point described the tangential contact between the patella and Ellipse 2. Mathematically, this meant that unit vectors $\vec{u}_{pat}$ and $\vec{u}_{fem2}$ were parallel and as a consequence, their cross product was equal to zero. This relationship was defined as follows:

$$\vec{u}_{pat} \times \vec{u}_{fem2} = 0 \tag{11}$$

Next, $\vec{u}_{pat}$ and $\vec{u}_{fem2}$ were defined mathematically in the global coordinate system:

$$\vec{u}_{pat} = \begin{bmatrix} sin\alpha \\ cos\alpha \\ 0 \\ 0 \end{bmatrix} \tag{12}$$

$$\vec{u}_{fem2} = \frac{1}{{A_2}^2 sin^2\alpha + {B_2}^2 cos^2\alpha} T_{tf} \begin{bmatrix} -A_2 \sin\Phi_2 \\ B_2 \cos\Phi_2 \\ 0 \\ 0 \end{bmatrix} \tag{13}$$

Combining (12), (13), and (14) produced the following equation, where the third element of the resulting vector formed the sixth element of the residual vector.

$$\begin{bmatrix} \boldsymbol{sin\alpha} \\ \boldsymbol{cos\alpha} \\ \mathbf{0} \\ \mathbf{0} \end{bmatrix} \times \frac{\mathbf{1}}{\boldsymbol{A_2}^2 \boldsymbol{sin^2\alpha} + \boldsymbol{B_2}^2 \boldsymbol{cos^2\alpha}} \boldsymbol{T_{tf}} \begin{bmatrix} -\boldsymbol{A_2}\mathbf{sin}\boldsymbol{\Phi_2} \\ \boldsymbol{B_2}\mathbf{cos}\boldsymbol{\Phi_2} \\ \mathbf{0} \\ \mathbf{0} \end{bmatrix} = \begin{bmatrix} \sim \\ \sim \\ \vec{\boldsymbol{R}}(\mathbf{6}) \\ \sim \end{bmatrix} \quad (\mathbf{14})$$

The three remaining equations described the geometric compatibility of the tibia and femur at the TF contact point. As with the PF contact point, it was assumed that tangential contact between the two surfaces occurred at a single point. In this case, the surface of Ellipse 1 was tangent to the tibial plateau. The close-up geometry of the TF contact point was described as follows:

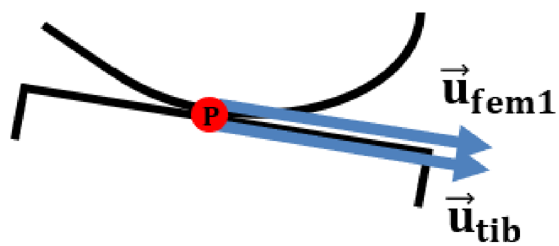


**Figure 5.** Close-up view of the TF contact point.

Where P represented the contact point, $\vec{u}_{tib}$ was the unit vector parallel to the tibial plateau, and $\vec{u}_{fem1}$ was the unit vector tangent to the surface of the femur. The agreement of the location of the contact point on the tibia and femur was described as follows:

$$P_{tib}(x, y) - P_{fem1}(x, y) = 0 \quad (15)$$

Then, both $P_{tib}$ and $P_{fem1}$ were mathematically defined in the global coordinate system using transformation matrix $T_{tf}$, yielding a vector whose first two elements formed the seventh and eighth elements of the residual vector.

$$\begin{bmatrix} \boldsymbol{Dsin\phi + (1 - P_{tp})L_{tp}cos\phi)} \\ \boldsymbol{Dcos\phi + (1 - P_{tp})L_{tp}sin\phi} \\ \mathbf{0} \\ \mathbf{0} \end{bmatrix} - \boldsymbol{T_{tf}} \begin{bmatrix} \boldsymbol{A_1 cos\Phi_1} \\ \boldsymbol{B_1 sin\Phi_1} \\ \mathbf{0} \\ \mathbf{0} \end{bmatrix} = \begin{bmatrix} \boldsymbol{\vec{R}(7)} \\ \boldsymbol{\vec{R}(8)} \\ \mathbf{0} \\ \mathbf{0} \end{bmatrix} \qquad \mathbf{(16)}$$

Where $T_{tf}$ was previously defined in (11).

The third equation derived at the TF contact point described the tangential contact between the tibial plateau and Ellipse 1. Mathematically, this meant that unit vectors , $\vec{u}_{tib}$ and $\vec{u}_{fem1}$ were parallel and as a consequence, their cross product was equal to zero. This relationship was defined as follows:

$$\vec{u}_{tib} \times \vec{u}_{fem1} = 0 \qquad (17)$$

Next, $\vec{u}_{tib}$ and $\vec{u}_{fem1}$ were defined mathematically in the global coordinate system:

$$\vec{u}_{tib} = \begin{bmatrix} cos\phi \\ -sin\phi \\ 0 \\ 0 \end{bmatrix} \qquad (18)$$

$$\vec{u}_{fem1} = T_{tf} \begin{bmatrix} -A_1 sin\Phi_1 \\ B_1 cos\Phi_1 \\ 0 \\ 0 \end{bmatrix} \qquad (19)$$

Combining (17), (18), and (19) produced the following equation, where the third element of the resulting four by one vector formed the ninth element of the residual vector.

$$\begin{bmatrix} \boldsymbol{cos\phi} \\ \boldsymbol{-sin\phi} \\ \mathbf{0} \\ \mathbf{0} \end{bmatrix} \times \boldsymbol{T_{tf}} \begin{bmatrix} \boldsymbol{-A_1 sin\Phi_1} \\ \boldsymbol{B_1 cos\Phi_1} \\ \mathbf{0} \\ \mathbf{0} \end{bmatrix} = \begin{bmatrix} \sim \\ \sim \\ \boldsymbol{\vec{R}(9)} \\ \sim \end{bmatrix} \qquad \mathbf{(20)}$$

Ultimately, nine equations were developed that defined the nine elements of the residual vector $\vec{R}$. These equations described the static equilibrium of the patella, the geometry of the PF contact point, and the geometry of the TF contact point. These nine equations were summarized as follows:

$$F_r \cos\alpha + F_{pl} sin\beta - F_q sin\theta = \vec{R}(1) \tag{3}$$

$$-F_r \sin\alpha + F_{pl} cos\beta - F_q cos\theta = \vec{R}(2) \tag{4}$$

$$\begin{bmatrix} -t \\ L_p - h \\ 0 \end{bmatrix} \times \begin{bmatrix} F_q \sin(\theta - \alpha) \\ F_q \cos(\theta - \alpha) \\ 0 \end{bmatrix} + \begin{bmatrix} -t \\ -h \\ 0 \end{bmatrix} \times \begin{bmatrix} F_{pl} \sin(\alpha - \beta) \\ F_{pl} \cos(\alpha - \beta) \\ 0 \end{bmatrix} = \begin{bmatrix} \sim \\ \sim \\ \vec{R}(3) \end{bmatrix} \tag{7}$$

$$\begin{bmatrix} -L_{tub} + L_{pl} + tcos\alpha + hsin\alpha \\ L_{pl}cos\beta - tsin\alpha + hcos\alpha \\ 0 \\ 0 \end{bmatrix} - T_{tf} \begin{bmatrix} C_x + A_2 cos\Phi_2 \\ C_y + B_2 sin\Phi_2 \\ 0 \\ 0 \end{bmatrix} = \begin{bmatrix} \vec{R}(4) \\ \vec{R}(5) \\ \sim \\ \sim \end{bmatrix} \tag{9}$$

$$\begin{bmatrix} sin\alpha \\ cos\alpha \\ 0 \\ 0 \end{bmatrix} \times \frac{1}{{A_2}^2 sin^2\alpha + {B_2}^2 cos^2\alpha} T_{tf} \begin{bmatrix} -A_2 \sin\Phi_2 \\ B_2 \cos\Phi_2 \\ 0 \\ 0 \end{bmatrix} = \begin{bmatrix} \sim \\ \sim \\ \vec{R}(6) \\ \sim \end{bmatrix} \tag{14}$$

$$\begin{bmatrix} Dsin\phi + (1 - P_{tp})L_{tp}cos\phi) \\ Dcos\phi + (1 - P_{tp})L_{tp}sin\phi \\ 0 \\ 0 \end{bmatrix} - T_{tf} \begin{bmatrix} A_1 cos\Phi_1 \\ B_1 sin\Phi_1 \\ 0 \\ 0 \end{bmatrix} = \begin{bmatrix} \vec{R}(7) \\ \vec{R}(8) \\ 0 \\ 0 \end{bmatrix} \tag{16}$$

$$\begin{bmatrix} cos\phi \\ -sin\phi \\ 0 \\ 0 \end{bmatrix} \times T_{tf} \begin{bmatrix} -A_1 sin\Phi_1 \\ B_1 cos\Phi_1 \\ 0 \\ 0 \end{bmatrix} = \begin{bmatrix} \sim \\ \sim \\ \vec{R}(9) \\ \sim \end{bmatrix} \tag{20}$$

After developing the system of equations, a custom solving and postprocessing script was written in MATLAB. First, the input parameters were defined. Next, the solving algorithm computed the solution to the system of equations and further processed the solution; this occurred once for each value of theta. Finally, after all solutions were computed and stored, the results of the simulation were displayed via an animation. These steps are summarized in the following flowchart:

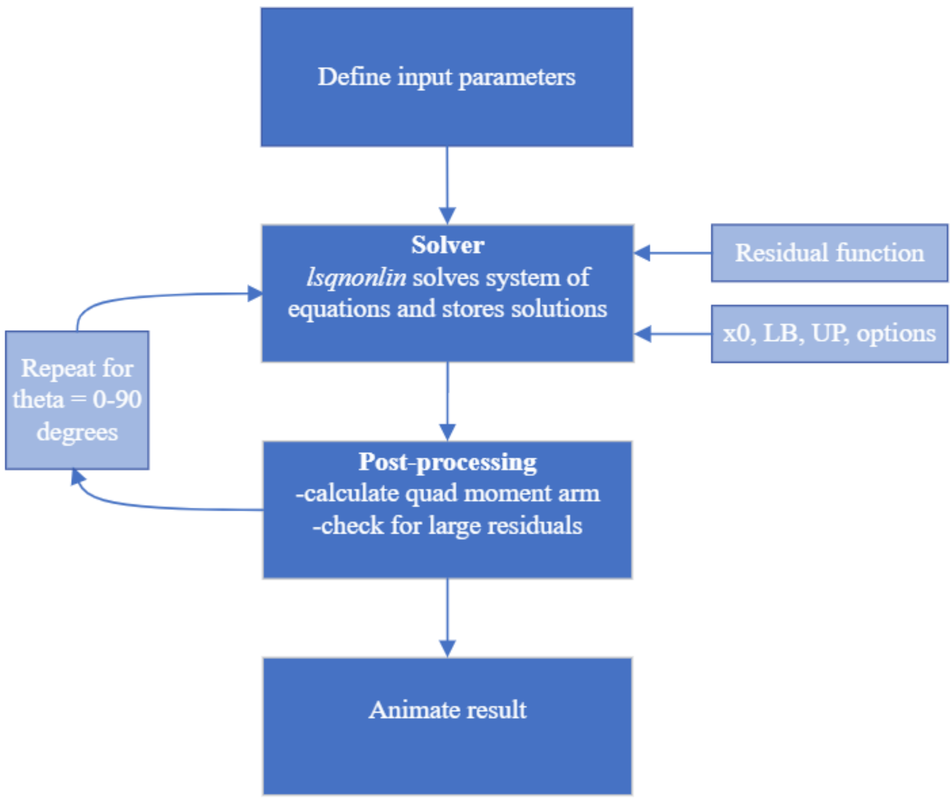


**Figure 6.** Overview of Natural Knee Model code.

MATLAB offered multiple built-in functions capable of solving systems of non-linear equations, and the function used in this model was *lsqnonlin*. *lsqnonlin* is a nonlinear least-squares solver that solves systems by minimizing the squared elements of the residual vector. In our case, the residual vector $\vec{R}$ was calculated by a residual function that contained the previously developed system of equations. This residual function was an input into *lsqnonlin*, which would use the function to solve the system of equations. In addition to the residual function, *lsqnonlin* had multiple input arguments, including "*x0*", "lower bound", "upper bound", and "options". *x0* was an initial guess provided to the solver so it could perform its analysis more efficiently. Each time the system of equations was solved, the solution vector would become the initial guess for the subsequent frame of the simulation. In addition, the "lower bound" and "upper bound" were vectors that provided a range of values for each unknown. *x0* and the bounds worked to increase efficiency and narrow the scope of the potential solutions considered by the solver. The final input into *lsqnonlin* was "options," which allowed more specific solver preferences to be specified. Within "options", the residual tolerance was set to 1e-6. This tolerance specified how close the solver had to get to a solution before moving onto the next frame. In this case, each element of $\vec{R}$ had to be less than 1e-6 in order for the solution to be valid. When this tolerance was reached, the corresponding solution vector was stored in a matrix for later use.

For each frame of the simulation, after the solution vector was calculated, the quadriceps effective moment $M_{eff}$ was calculated. $M_{eff}$ was a metric developed by Yamaguchi and Zajac [5] to describe the overall leverage and mechanical advantage of the extensor mechanism. The force that extends the knee begins in the quadriceps, is transmitted by the patella, and ultimately applied by the patellar ligament. Therefore, it was useful to have a moment arm that, when multiplied by the quadriceps force, yielded the moment about the joint. The definition of $M_{eff}$ was based on this moment balance about the TF contact point:

$$F_q M_{eff} = F_{pl} M_{act} \tag{21}$$

Where $F_q$ and $F_{pl}$ are the quadriceps and patellar ligament forces, and $M_{act}$ is the "actual" moment arm of the patellar ligament force about the TF contact point. Therefore, $M_{eff}$ was defined as follows:

$$M_{eff} = \frac{F_{pl} M_{act}}{F_q} \tag{22}$$

$M_{eff}$ was computed at every frame of the simulation during the post-processing of each solution. $F_q$ was an input to the model, $F_{pl}$ was an unknown determined by lsqnonlin, and $M_{act}$ was calculated as the perpendicular distance between the patellar ligament and TF contact point.

After post-processing the model's output, the results of the simulation were displayed by an animation. The animation used the aforementioned solution matrix to draw the patella, femur, tibia, and other knee elements at each frame. The resulting animation was a useful tool for verifying that the model was functioning as intended and producing physically meaningful results. In addition, the animation feature helped to visualize how structural changes to the knee affect its function.

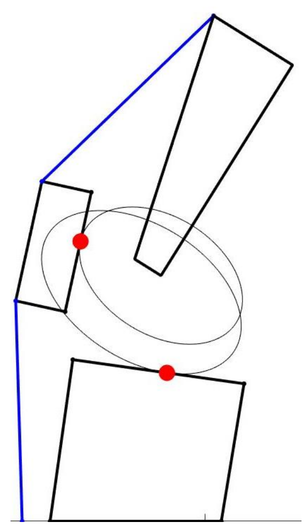

**Figure 7.** Image from an animation of the Natural Knee Model.

Once the Natural Knee Model was verified to be performing as intended, it was implemented to study Osgood Schlatter (OS) Disease. Two characteristic structural changes that accompany OS are a lengthening of the tibial tubercle and patella alta. Tubercle length was already an input parameter to the model, and patella alta was simulated by adjusting the length of the patellar ligament. A sensitivity analysis was employed in which the model was run multiple times, varying the two parameters of interest. The tubercle length was varied from 0 to 10mm in steps of 1mm, in accordance with measurements by Lee et al. [35], and the patellar ligament length was varied from 6.5cm to 7.2cm in steps of 0.07cm, a range of values obtained from Grelsamer et al. [22].

### 3.2 Hinged TKR Model

The Hinged TKR Model shared many similarities with the Natural Knee Model but had certain key distinctions. Like the previous model, the Hinged TKR Model was two dimensional and modeled rigid bodies in the sagittal plane. As the name suggests, this model simulated a commercially available hinged knee replacement, the type of implant that is commonly used in revision surgery. Once the model was developed, a sensitivity analysis was performed to assess the impact of various design criteria. Like in the Natural Knee Model, a system of equations was developed to describe the equilibrium and geometry of the knee. A more generalized approach was taken for these equations, in which the patella and femoral condyle surfaces were modeled as parameterized splines based on data from the real-world implant. The tibia was not modeled beyond the hinge, which was fixed in the sagittal plane and took the place of the TF contact point described in the Natural Knee Model.

The Hinged TKR Model was based on a system of seven equations, three describing the equilibrium of the patella, three describing the PF contact point, and one describing the constant length of the patellar ligament. The system was solved from 0 to 90 degrees in increments of 0.2 degrees, and solutions at every frame were stored for subsequent processing.

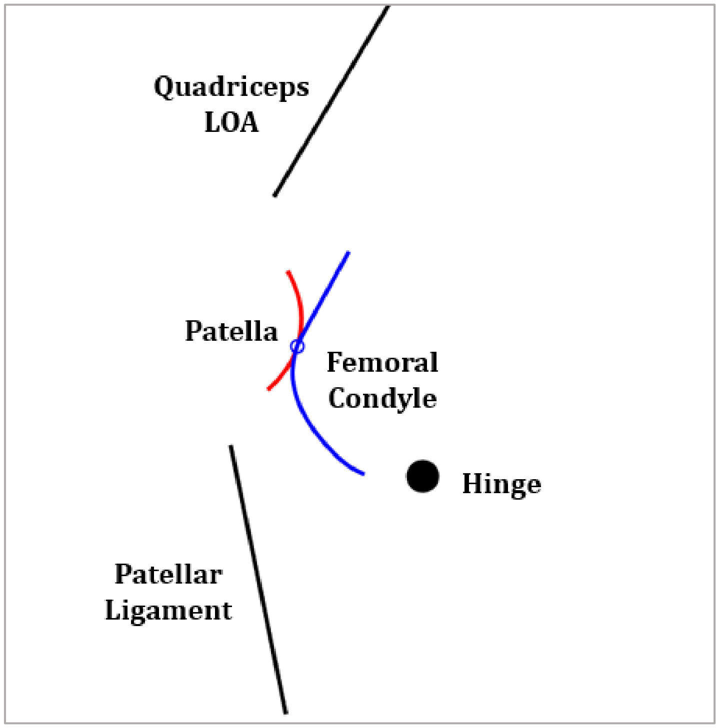


**Figure 8.** Simplified representation of the Hinged TKR Model, with the major components labeled.

As demonstrated by Figure 8, the geometries of the knee and implant were greatly simplified and only included elements necessary for the simulation. The patella and femoral condyle surfaces were representative of the real-world implant, as point coordinates along the surfaces were selected in the implant CAD file and imported into MATLAB where they were interpolated to create two continuous splines. Locations along the patellar and femur splines were specified by the parameter $t$, where a point $P(x,y)$ along either spline was described simply as $(x(t), y(t))$. Derivatives of the splines were also obtained, and the line tangent to a spline at a given parameter $t$ was given by $(x'(t), y'(t))$.

The origin of the global coordinate system was defined at the insertion point of the patellar ligament on the tibia, which remained fixed, while the origin of the local femoral coordinate system was defined at the center of the hinge. Additionally, a local patellar coordinate system was established; its origin did not have particular anatomical significance, but its location was recorded to allow transformations between coordinate systems. These three coordinate systems were summarized as follows:

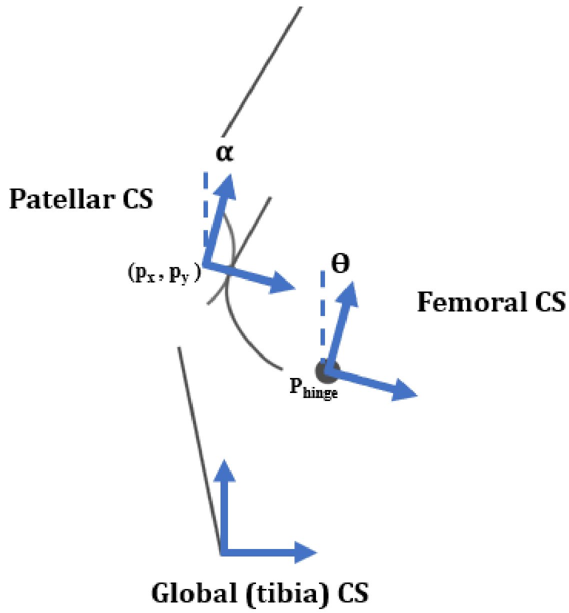


**Figure 9.** Diagram representing the global, femoral, and patellar coordinate systems.

Like the Natural Knee Model, the Hinged TKR Model required multiple input parameters to describe the precise geometry of the knee joint. Much of the input data was obtained by making measurements on the physical implant using a motion capture system. In this case, measurements were made in each point's local coordinate system and transformed to the global coordinate system as necessary. Distances were measured in centimeters, angles in degrees, and forces in Newtons. The input parameters were as follows:

**Table 3.** Nominal input parameters of the Hinged TKR Model. These inputs described knee geometry and mathematical parameters necessary to develop the system of equations. Coordinate system is abbreviated “CS”.

| *Symbol* | *Definition* | *Value* | *Notes* |
|---|---|---|---|
| $\boldsymbol{\theta}$ | Flexion of the femur relative to the tibial axis. Referred to as “knee flexion angle”. | 0-90 degrees | Varied at one-degree increments. |
| $\mathbf{F_q}$ | Quadriceps force | 250 N | |
| $\mathbf{L_{pl}}$ | Patellar ligament length | 6.52 cm | |
| $\vec{\boldsymbol{P}}_{\boldsymbol{pl_{orig}}}$ | Origin of patellar ligament in patellar CS | (-0.401, 3.31, 0) | Each of these points were recorded in a certain CS depending on if the point was on the patella, femur, or tibia. |
| $\vec{\boldsymbol{P}}_{\boldsymbol{pl_{ins}}}$ | Insertion of patellar ligament in global CS | (0, 0, 0) | |
| $\vec{\boldsymbol{P}}_{\boldsymbol{hinge}}$ | Location of hinge in global CS | (3.45, 6.00, 0) | |
| $\vec{\boldsymbol{P}}_{\boldsymbol{q_{orig}}}$ | Origin of quadriceps in femoral CS | (-4.10, 58.22, 0) | |
| $\vec{\boldsymbol{P}}_{\boldsymbol{q_{ins}}}$ | Insertion of quadriceps in patellar CS | (-0.36, 3.31, 0) | |

These input parameters were used to define the system of seven equations describing the Hinged TKR Model. The seven equations described the equilibrium of the patella, the geometry of the PF contact point, and the constant length of the patellar ligament. As with the previous model, each of the equations was set equal to a residual, and the set of seven residuals formed the residual vector $\vec{R}$. The solver *lsqnonlin* solved the system at each flexion angle by minimizing $\vec{R}$. The unknowns in this system included the angle of the patella, origin of the patellar coordinate system, PF contact point parameters on the patella and femur splines, as well as the PF contact force and patellar ligament force. These unknowns are summarized as follows:

**Table 4.** The seven unknown variables of the Hinged TKR Model.

| *Symbol* | *Definition* |
|---|---|
| $\mathbf{t_p}$ | Parameter of patellar spline at which PF contact point occurs. |
| $\mathbf{t_f}$ | Parameter of femoral spline at which PF contact point occurs |
| $\boldsymbol{\alpha}$ | Patellar CS orientation with respect to global vertical axis |
| $\mathbf{p_x}, \mathbf{p_y}$ | Location of patellar CS origin in global CS |
| $\mathbf{F_r}$ | Patellofemoral contact force |
| $\mathbf{F_{pl}}$ | Patellar ligament force |

After defining the assumptions, input parameters, and unknowns, the system of equations describing the Hinged TKR Model was developed. Keeping with the same format as the Natural Knee Model, equations describing elements of $\vec{R}$ will be bolded.

First, two transformation matrices were defined in order to transform points in the femoral and patellar coordinate systems to the global coordinate system. The matrices were named $T_{tf}$ and $T_{tp}$, respectively.

$$T_{tf} = \begin{bmatrix} cos\theta & sin\theta & 0 & P_{hinge_x} \\ -sin\theta & cos\theta & 0 & P_{hinge_y} \\ 0 & 0 & 1 & 0 \\ 0 & 0 & 0 & 0 \end{bmatrix} \tag{23}$$

$$T_{tp} = \begin{bmatrix} cos\theta & sin\theta & 0 & t_x \\ -sin\theta & cos\theta & 0 & t_y \\ 0 & 0 & 1 & 0 \\ 0 & 0 & 0 & 0 \end{bmatrix} \tag{24}$$

In addition, the three forces, $F_q$, $F_r$, *and* $F_{pl}$, were defined using vectors in the global coordinate system. Each vector was formed by multiplying the magnitude of the force by a unit vector in the direction of the force. The unit vectors for $\overrightarrow{F_q}$ and $\overrightarrow{F_{pl}}$ were found using the coordinates of the origins and insertions of the quadriceps force and patellar ligament. In the case of $\overrightarrow{F_r}$, the unit vector was defined as inward normal to the spline at the PF contact point. All coordinates were first transformed to the global coordinate system using the aforementioned transformation matrices. The vectors were defined as follows:

$$\overrightarrow{F_q} = F_q\left(\frac{\vec{\boldsymbol{P}}_{\boldsymbol{q_{orig}}} - \vec{\boldsymbol{P}}_{\boldsymbol{pl_{ins}}}}{\left\|\vec{\boldsymbol{P}}_{\boldsymbol{q_{orig}}} - \vec{\boldsymbol{P}}_{\boldsymbol{pl_{ins}}}\right\|}\right) \tag{25}$$

$$\overrightarrow{F_{pl}} = F_{pl}\left(\frac{\vec{\boldsymbol{P}}_{\boldsymbol{pl_{ins}}} - \vec{\boldsymbol{P}}_{\boldsymbol{pl_{orig}}}}{\left\|\vec{\boldsymbol{P}}_{pl_{ins}} - \vec{\boldsymbol{P}}_{\boldsymbol{pl_{orig}}}\right\|}\right) \tag{26}$$

$$\overrightarrow{F_r} = F_r\begin{bmatrix}-y'(t_p)\\ x'(t_p)\end{bmatrix} \tag{27}$$

The first three equations of the system were developed by invoking the static equilibrium of the patella. That is, at any given knee flexion angle, it was assumed that the forces on the patella were balanced according to Figure 3, the only difference being the curvature of the patella. This equilibrium assumption yielded three equations, two describing static equilibrium in the x- and y- directions, and one describing the rotational static equilibrium. The first two elements of $\vec{R}$ were defined as follows:

$$\overrightarrow{\boldsymbol{F_q}} + \overrightarrow{\boldsymbol{F_{pl}}} + \overrightarrow{\boldsymbol{F_r}} = \begin{bmatrix}\vec{\boldsymbol{R}}(\mathbf{1})\\ \vec{\boldsymbol{R}}(\mathbf{2})\\ \sim\end{bmatrix} \tag{28}$$

The third element of $\vec{R}$, describing rotational equilibrium, was then derived as follows:

$$\vec{M}_q + \vec{M}_{pl} + \vec{M}_r = 0 \tag{29}$$

$$\begin{bmatrix} \boldsymbol{P}_{q_{ins_x}} \\ \boldsymbol{P}_{q_{ins_y}} \\ \boldsymbol{0} \end{bmatrix} \times \vec{\boldsymbol{F}}_{\boldsymbol{q}} + \begin{bmatrix} \boldsymbol{P}_{pl_{orig_x}} \\ \boldsymbol{P}_{pl_{orig_y}} \\ \boldsymbol{0} \end{bmatrix} \times \vec{\boldsymbol{F}}_{\boldsymbol{pl}} + \begin{bmatrix} \boldsymbol{x}_{\boldsymbol{pat}}(\boldsymbol{t}_{\boldsymbol{p}}) \\ \boldsymbol{y}_{\boldsymbol{pat}}(\boldsymbol{t}_{\boldsymbol{p}}) \\ \boldsymbol{0} \end{bmatrix} \times \overrightarrow{\boldsymbol{F}_{\boldsymbol{r}}} = \begin{bmatrix} \sim \\ \sim \\ \vec{\boldsymbol{R}}(\boldsymbol{3}) \end{bmatrix} \tag{30}$$

Where all coordinates were first transformed to the global coordinate system and "~" is used to indicate a vector element that is not included in the residual vector.

The next three elements of $\vec{R}$ described the geometric compatibility of the patella and femur at the PF contact point. Using the same assumptions of contact points in the Natural Knee Model, the equations stated that 1) The point defined on the patella spline had the same coordinates as the point defined on the femur spline and 2) The two segments could not pass through each other. The agreement of the location of the contact point on the patella and femur splines was described as follows:

$$P_{pat}(x, y) - P_{fem}(x, y) = 0 \tag{31}$$

$$\begin{bmatrix} \boldsymbol{x}_{\boldsymbol{pat}}(\boldsymbol{t}_{\boldsymbol{p}}) \\ \boldsymbol{y}_{\boldsymbol{pat}}(\boldsymbol{t}_{\boldsymbol{p}}) \end{bmatrix} - \begin{bmatrix} \boldsymbol{x}_{\boldsymbol{fem}}(\boldsymbol{t}_{\boldsymbol{f}}) \\ \boldsymbol{y}_{\boldsymbol{fem}}(\boldsymbol{t}_{\boldsymbol{f}}) \end{bmatrix} = \begin{bmatrix} \vec{\boldsymbol{R}}(\boldsymbol{4}) \\ \vec{\boldsymbol{R}}(\boldsymbol{5}) \end{bmatrix} \tag{32}$$

The other equation derived at the PF contact point described the tangential contact between the patella and femur. Mathematically, this meant that the derivatives of the splines were parallel at the contact point and the third element of their cross product was equal to zero. Understanding this relationship, the sixth element of $\vec{R}$ was defined as follows:

$$\begin{bmatrix} \boldsymbol{x}_{\boldsymbol{fem}}'(\boldsymbol{t}_{\boldsymbol{f}}) \\ \boldsymbol{y}_{\boldsymbol{fem}}'(\boldsymbol{t}_{\boldsymbol{f}}) \\ \boldsymbol{0} \end{bmatrix} \times \begin{bmatrix} \boldsymbol{x}'_{\boldsymbol{pat}}(\boldsymbol{t}_{\boldsymbol{p}}) \\ \boldsymbol{y}'_{\boldsymbol{pat}}(\boldsymbol{t}_{\boldsymbol{p}}) \\ \boldsymbol{0} \end{bmatrix} = \begin{bmatrix} \sim \\ \sim \\ \vec{\boldsymbol{R}}(\boldsymbol{6}) \end{bmatrix} \tag{33}$$

The seventh and final element of $\vec{R}$ described the constant length of the patellar ligament, which was necessary to further constrain the knee joint and model the desired motion. This equation was defined as follows:

$$\left\| \begin{bmatrix} \boldsymbol{P_{pl_{orig_x}}} \\ \boldsymbol{P_{pl_{orig_y}}} \end{bmatrix} - \begin{bmatrix} \boldsymbol{P_{pl_{ins_x}}} \\ \boldsymbol{P_{pl_{ins_y}}} \end{bmatrix} \right\| - \boldsymbol{L_{pl}} = \vec{\boldsymbol{R}}(\boldsymbol{7}) \qquad (\boldsymbol{34})$$

With that, seven equations had been developed, summarized as follows:

$$\overrightarrow{F_q} + \overrightarrow{F_{pl}} + \overrightarrow{F_r} = \begin{bmatrix} \vec{R}(1) \\ \vec{R}(2) \\ 0 \end{bmatrix} \qquad (28)$$

$$\begin{bmatrix} P_{q_{ins_x}} \\ P_{q_{ins_y}} \\ 0 \end{bmatrix} \times \vec{F}_q + \begin{bmatrix} P_{pl_{orig_x}} \\ P_{pl_{orig_y}} \\ 0 \end{bmatrix} \times \vec{F}_{pl} + \begin{bmatrix} x_{pat}(t_p) \\ y_{pat}(t_p) \\ 0 \end{bmatrix} \times \overrightarrow{F_r} = \begin{bmatrix} \sim \\ \sim \\ \vec{R}(3) \end{bmatrix} \qquad (30)$$

$$\begin{bmatrix} x_{pat}(t_p) \\ y_{pat}(t_p) \end{bmatrix} - \begin{bmatrix} x_{fem}(t_f) \\ y_{fem}(t_f) \end{bmatrix} = \begin{bmatrix} \vec{R}(4) \\ \vec{R}(5) \end{bmatrix} \qquad (32)$$

$$\begin{bmatrix} x_{fem}'(t_f) \\ y_{fem}'(t_f) \\ 0 \end{bmatrix} \times \begin{bmatrix} x'_{pat}(t_p) \\ y'_{pat}(t_p) \\ 0 \end{bmatrix} = \begin{bmatrix} \sim \\ \sim \\ \vec{R}(6) \end{bmatrix} \qquad (33)$$

$$\left\| \begin{bmatrix} P_{pl_{orig_x}} \\ P_{pl_{orig_y}} \end{bmatrix} - \begin{bmatrix} P_{pl_{ins_x}} \\ P_{pl_{ins_y}} \end{bmatrix} \right\| - L_{pl} = \vec{R}(7) \qquad (34)$$

As with the Natural Knee Model, a custom solving and postprocessing script was written in MATLAB that defined inputs, solved the system at each flexion angle using *lsqnonlin*, processed the solution, and displayed the results using an animation. In addition, a residual function that contained the above equations computed $\vec{R}$ and served as an input to *lsqnonlin.* Other inputs included “x0”, “lower bound”, “upper bound”, and “options”, which were previously discussed.

At each frame of the simulation, the quadriceps effective moment arm, $M_{eff,}$ was calculated using the following equation, which was previously defined in the discussion of the Natural Knee Model:

$$M_{eff} = \frac{F_{pl} M_{act}}{F_q} \tag{22}$$

Where $F_q$ was an input to the simulation, $F_{pl}$ was calculated at each frame, and $M_{act}$ was the perpendicular distance from the hinge to the patellar ligament. To review, $M_{eff}$ was a metric developed to measure the overall mechanical advantage of the quadriceps force, taking into account the leveraging action of the patella. As with the Natural Knee Model, an animation was generated at the conclusion of the simulation to visualize the model's output and verify it was functioning as intended.

After the Hinged TKR Model was verified, it was implemented to study two technical design considerations pertaining to hinged knee replacements— the location of the joint line and the anterior-posterior (A-P) position of the hinge. The location of the joint line was varied by adjusting the length of the patellar ligament, $L_{pl}$. In practice, the joint line is determined by the resections of the tibia and femur; however, for the purposes of this 2D simulation, it was assumed this structural change could be modeled by varying $L_{pl}$. In addition, the A-P position of the hinge was varied by adjusting the x-coordinate of $P_{hinge}$, that is, the location of the hinge in the global coordinate system. $P_{hinge\_x}$ was increased and decreased by 0.5cm in steps of 0.5cm from its nominal value of 3.45cm, which was an arbitrary choice based on the hinge diameter. $L_{pl}$ was varied from 0.5cm to 7.2cm in steps of .07cm, a range of values obtained from Grelsamer at al. [22]. As these two quantities were varied, their impact on $M_{eff}$ and PF contact force $F_r$ was studied.

### 3.3 Hinged TKR Model with Knee Simulator Input

The third and final 2D model developed for this study was an extension of the Hinged TKR Model that included input from the Penn State Knee Simulator (PSKS), which obtained realistic input data for the model. In addition, the PSKS was used to evaluate the agreement between the computer model and benchtop testing data. The PSKS was a non-cadaveric Oxford Rig-style knee simulator that modeled knee extension under load. Driven by a linear actuator that acted as the quadriceps, the PSKS featured a commercially available hinged knee replacement and two load cells that measured the quadriceps force and three-dimensional PF contact force.

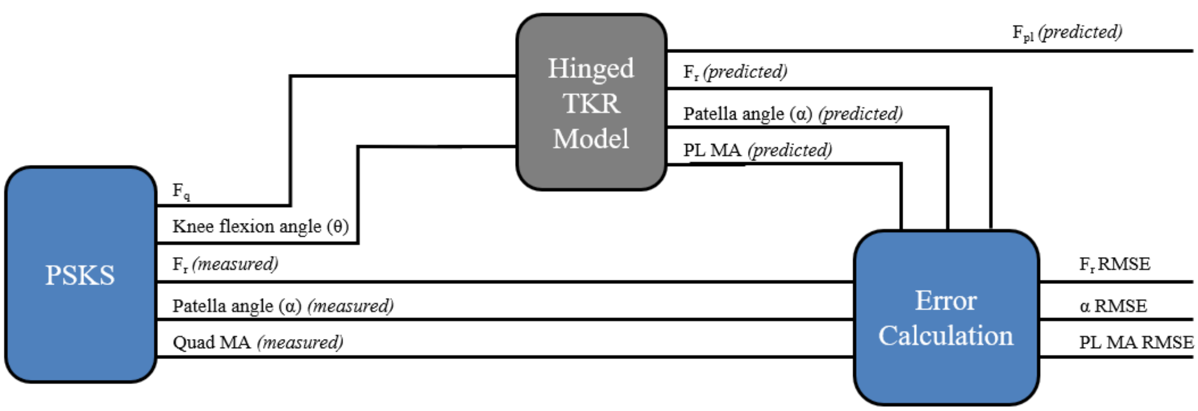


**Figure 10.** Overview of the Hinged TKR Model with Knee Simulator Input.

An overview of the Hinged TKR Model with Knee Simulator Input is given as follows:

As shown in Figure 10, the PSKS measured quadriceps force $F_q$ at each flexion angle, and this data was fed into the Hinged TKR Model. The PSKS also measured PF contact force $F_r$, patellar angle $\alpha$, and patellar ligament moment arm $MA_{pl}$, referred to as $MA_{act}$ in prior calculations. Informed by the knee simulator input, the Hinged TKR Model was run, calculating values for $F_r$, $\alpha$, and $MA_{pl}$. The agreement between the experimental and predicted values was quantified using a Root Mean Square Error (RMSE) calculation, a statistical tool that represents the standard deviation of the prediction errors. In total, five simulation trials were performed using the PSKS and five corresponding simulations were performed using the Hinged TKR Model.

# Chapter 4

# Results

## 4.1 Natural Knee Model

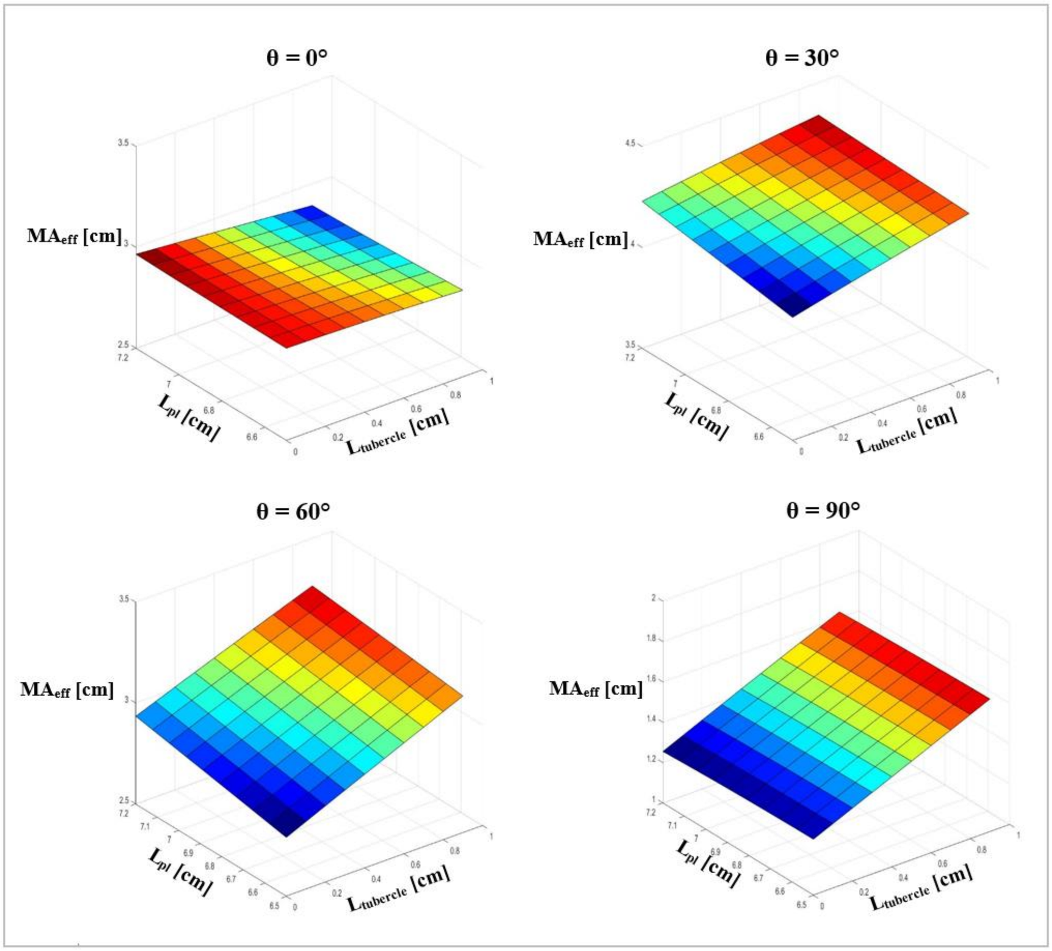


**Figure 11.** Quadriceps effective moment arm as a function of tibial tubercle length and patellar ligament length, shown at knee flexion angles of 0, 30, 60, and 90 degrees.

The quadriceps effective moment arm increased with tubercle length and patellar ligament length at flexion angles of 30° and greater (Figure 11). The magnitude of the effect of these structural changes was indicated by the slope of each surface plot, and the most pronounced effect was seen at $\theta = 60°$. $MA_{eff}$ appeared linearly proportional to $L_{tubercle}$ and $L_{pl}$ when these values were varied of independent of each other. When varied at the same time, their individual impacts on $MA_{eff}$ were compounded. This relationship was most apparent at the maximum value of the $\theta = 60°$ plot, where an increase in $L_{tubercle}$ from 0 to 1cm and an increase in $L_{pl}$ from 6.5cm to 7.2cm (10.8%) combined to produce an increase in $MA_{eff}$ from 2.79cm to 3.27cm (17.2%). $L_{tubercle}$ and $L_{pl}$ had a similar impact on $MA_{eff}$ at $\theta = 30°$ and $\theta = 90°$, while there was virtually no impact at $\theta = 0°$.

## 4.2 Hinged TKR Model

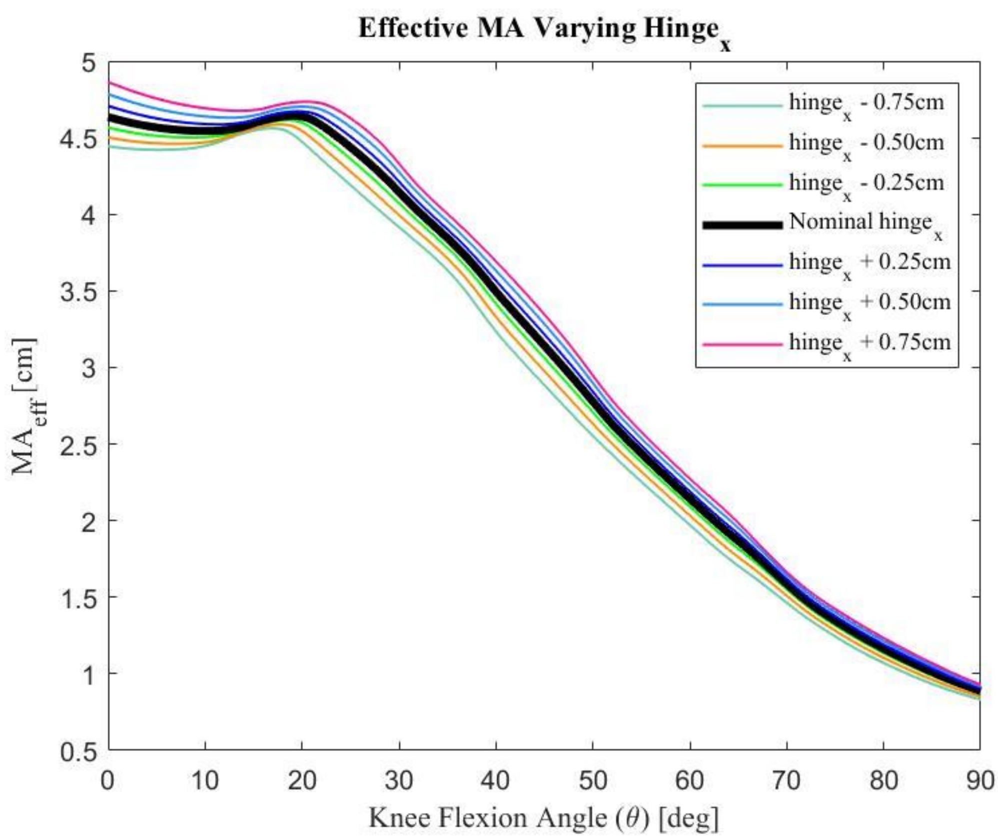


**Figure 12.** Quadriceps effective moment arm as a function of knee flexion angle and A-P position of the hinge.

Quadriceps effective moment arm decreased with a more anterior hinge and increased with a more posterior hinge (Figure 12). This relationship was most pronounced at flexion angles from 0 to 20 degrees and gradually became less pronounced as flexion angle increased from 20 to 90 degrees. The greatest increase in $MA_{eff}$ occurred when $hinge_x$ was increased by 0.75cm, while the greatest decrease in $MA_{eff}$ occurred when $hinge_x$ was decreased by 0.75cm. Overall, the curves representing modified hinge position closely followed the nominal hinge curve.

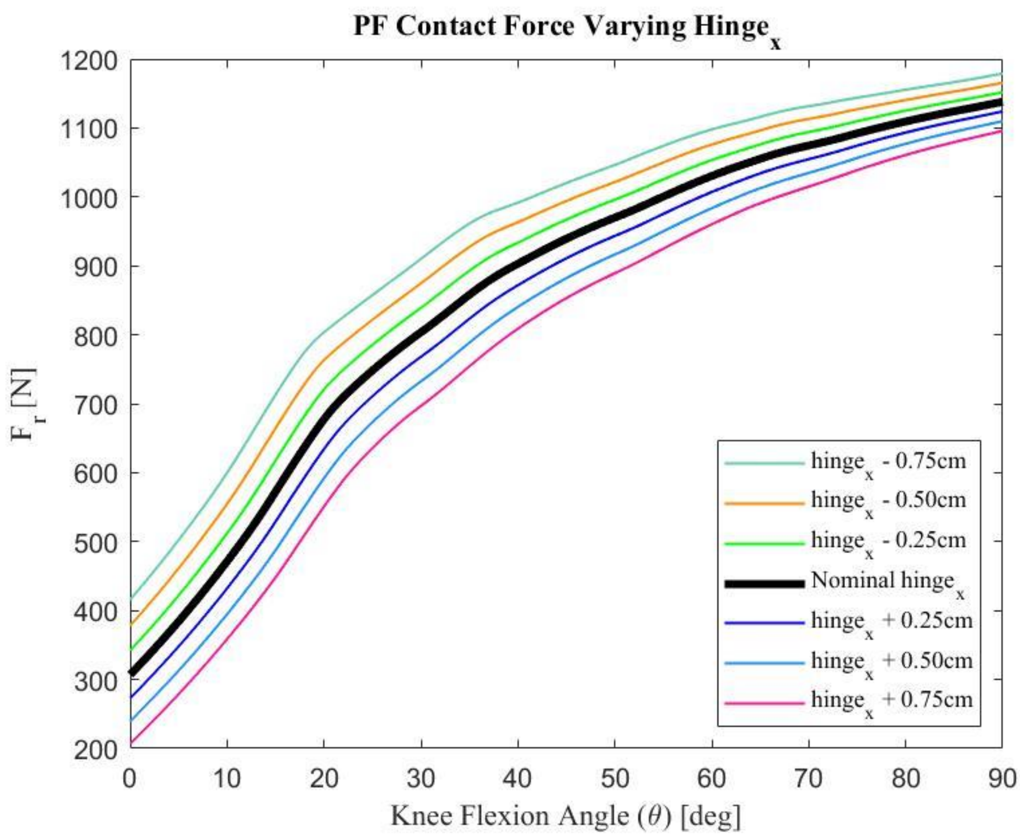


**Figure 13.** Patellofemoral contact force as a function of knee flexion angle and A-P position of the hinge. The nominal x-position of the hinge was 3.45cm in the global coordinate system.

Patellofemoral contact force increased with a more anterior hinge and decreased with a more posterior hinge (Figure 13). The impact of A-P hinge position remained relatively consistent across flexion angles from 0 to 90 degrees, indicated by the even spacing between the curves. The variation of the x-position of the hinge had a significant effect on $F_r$. For example, At $\theta = 0°$, a 21.7% decrease in $hinge_x$ produced a 35.5% in $F_r$, and a 21.7% increase in $hinge_x$ produced a 31.8% decrease in $F_r$, when compared to the nominal value.

### 4.3 Hinged TKR Model with Knee Simulator Input

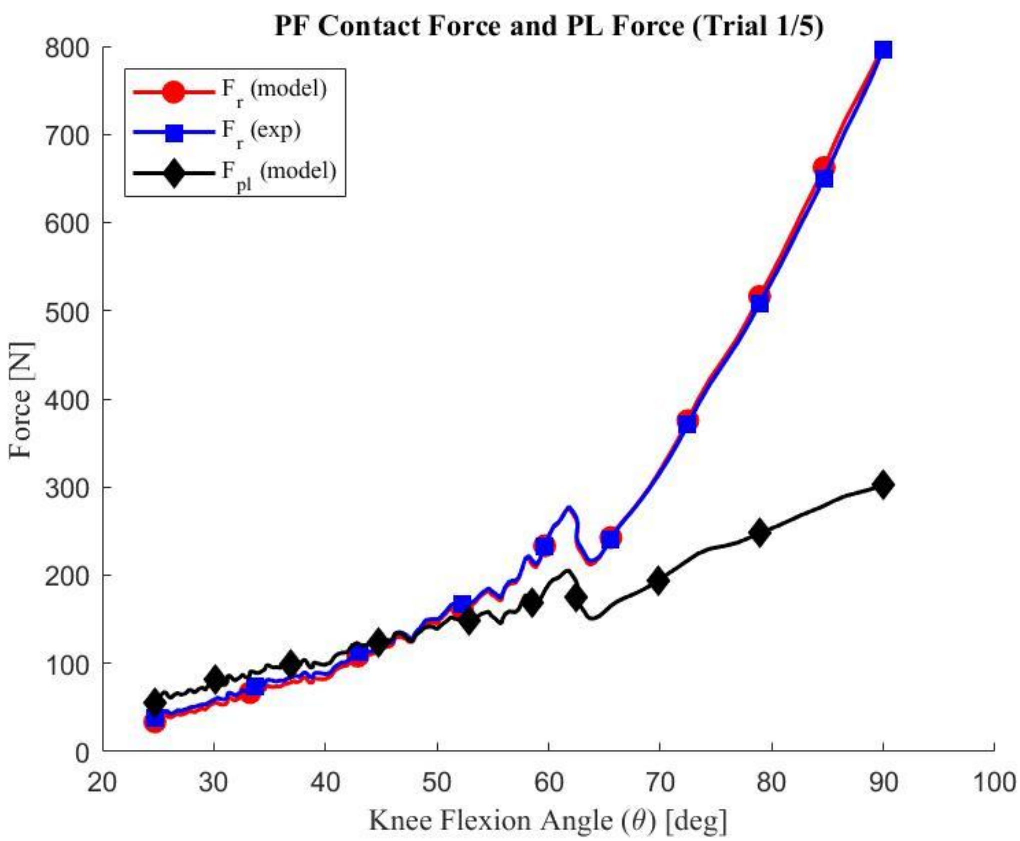


**Figure 14.** Predicted PF contact force, experimental contact force, and predicted patellar ligament force, all as a function of knee flexion angle. This data was collected during the first of the five trials.

The patellofemoral contact force predicted by the model closely agreed with the values measured experimentally in the PSKS (Figure 14). The agreement was consistent across flexion angles from 0 to 90 degrees. In addition, the patellar ligament force was predicted by the model and increased steadily with flexion angle. The mean RMS error of the predicted measurement across the five trials was 10.78N, and the standard deviation of the RMS error was 3.28N.

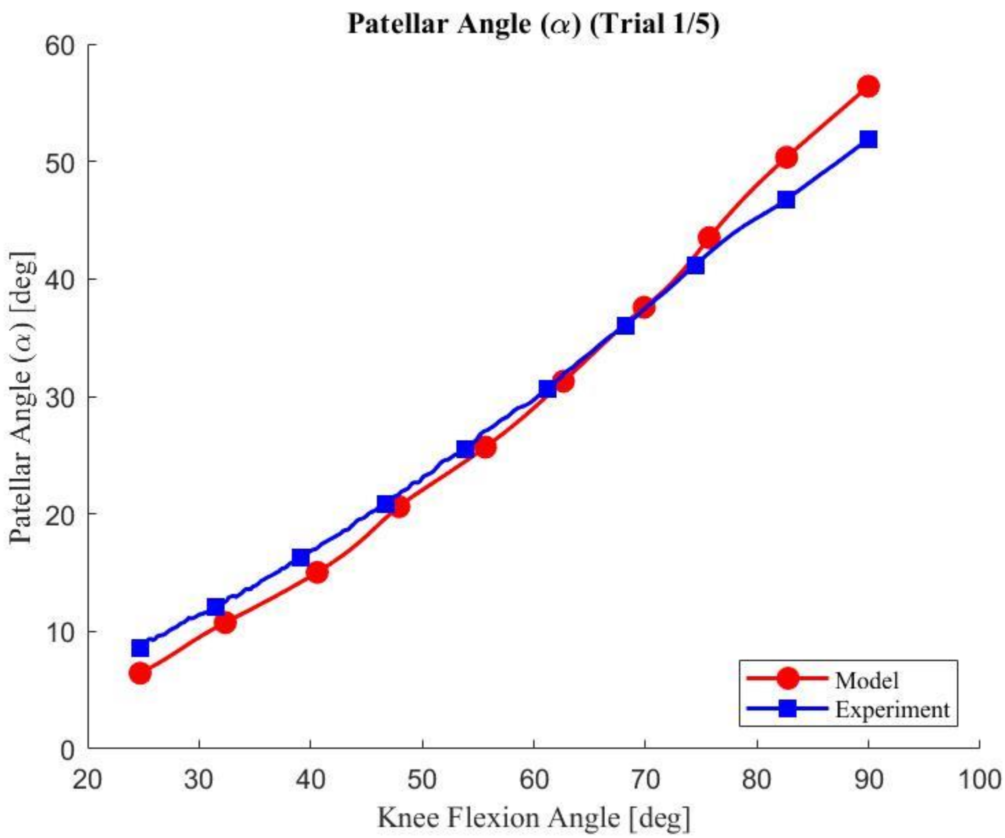


**Figure 15.** Predicted patellar angle and experimental patellar angle, as a function of knee flexion angle. This data was collected during the first of the five trials.

The patellar angle predicted by the model agreed with the values measured experimentally in the PSKS (Figure 15). The agreement was relatively consistent across flexion angles from 0 to 90 degrees and decreased slightly between 75 and 90 degrees. The proportionality between patellar angle and flexion angle was roughly linear, with the predicted curve having a slightly greater slope than the experimental curve. The mean RMS error of the predicted measurement across the five trials was 1.88 degrees, and the standard deviation of the RMS error was 0.038 degrees.

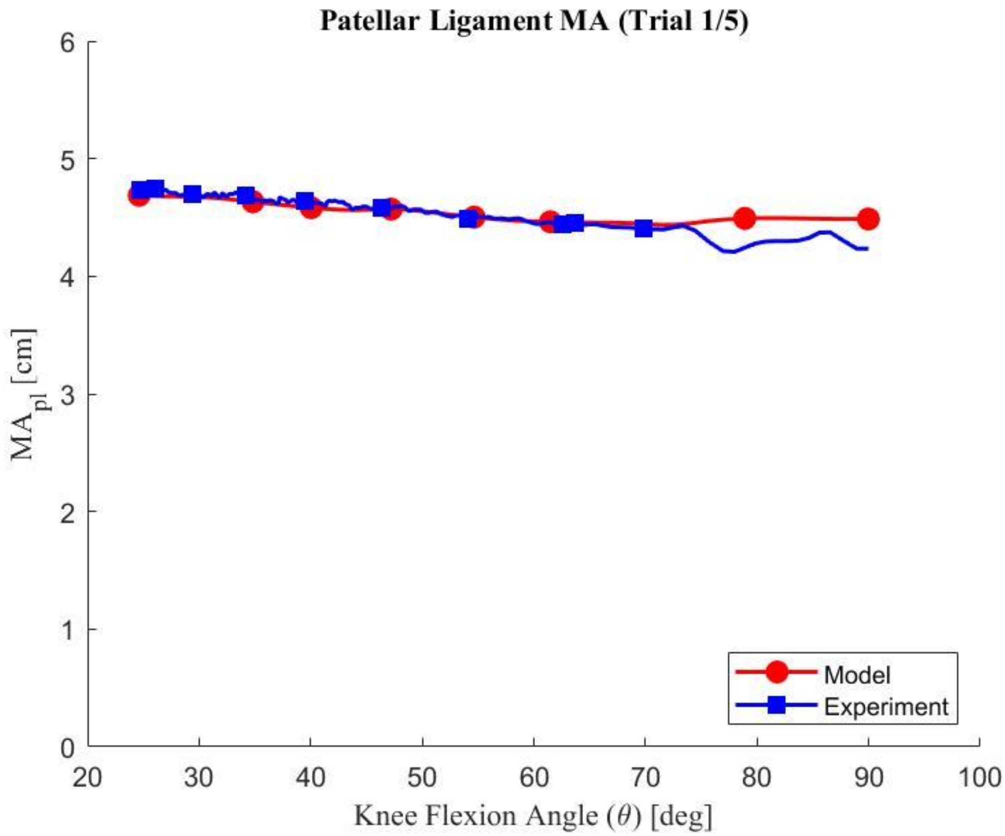


**Figure 16.** Predicted patellar ligament moment arm, and experimental patellar ligament moment arm, as a function of knee flexion angle. This data was collected during the first of the five trials.

The patellar ligament moment arm predicted by the model closely agreed with the values measured experimentally in the PSKS (Figure 16). The agreement was consistent across flexion angles from 0 to 90 degrees. Slight fluctuations in the experimental curve were seen from 75 to 90 degrees. The mean RMS error of the predicted measurement across the five trials was 0.049cm, and the standard deviation of the RMS error was 0.0056cm.

**Table 5.** Summary of Mean RMS Error and Standard Deviation of RMS Error for experimental vs. predicted measurements of PF contact force, patellar angle, and patellar ligament moment arm.

| | ***Mean RMS Error*** | ***Standard Deviation of RMS Error*** |
|---|---|---|
| **PF Contact Force** | 10.78 N | 3.28 N |
| **Patellar Angle** | 1.88 deg. | 0.038 deg. |
| **Patellar Ligament MA** | 0.049 cm | 0.0056 cm |

Overall, the RMS Errors of the predicted PF contact force, patellar angle, and patellar ligament moment arm were small compared to the magnitudes of the quantities themselves (Table 4). There was consistent agreement between predicted and experimental values, and the predicted curves were slightly smoother than the experimental curves.

# Chapter 5

# Discussion

## 5.1 Summary of Key Results

The Natural Knee Model, Hinged TKR Model, and Hinged TKR Model with Knee Simulator Input each produced their own findings and shed light on the mechanics of the knee extensor mechanism. The Natural Knee Model was an extension of the work of Yamaguchi and Zajac [5] and characterized the impact of Osgood-Schlatter disease on knee mechanics. Our study found that increased tibial tubercle length and patellar ligament length, two common effects of O-S, increased quadriceps effective moment arm; in fact, the effects of these two structural changes compounded when both were present. In addition, the Hinged TKR Model applied the planar equilibrium modeling paradigm of the Natural Knee Model to study a design consideration in hinged knee replacements. Using the geometry of a commercially available implant, this model revealed the impact of the anterior-posterior position of the hinge on quadriceps effective moment arm and patellofemoral contact force. Our study found that a more posterior hinge can decrease patellofemoral contact force and increase quadriceps moment arm. This model was used to make measurements that would have otherwise been impossible *in vivo* due to practical and ethical limitations. Finally, the Hinged TKR Model with Knee Simulator Input demonstrated that, with the right input data, a planar knee model can accurately predict the dynamics of the knee. Specifically, we used the measured quadriceps as an input to the model, which in turn predicted patellofemoral contact force, patellar angle, and patellar ligament moment arm. During this portion of the study, excellent agreement was found between experimental and predicted values, which spoke to the potential utility of planar equilibrium models in the design of knee replacement implants. This study was novel in that it was the first to augment an Oxford rig-style knee simulator with a planar equilibrium model to study hinged TKR implants.

## 5.2. Comparison to Previous Research

The findings of the Natural Knee Model were consistent with findings of Yamaguchi and Zajac [5] with respect to patellar ligament length providing support for the verification of the present model. Their study found that a 20% increase in patellar ligament length produced a significantly greater quadriceps effective moment arm at flexion angles beyond 15 degrees, which was consistent with our results. Similarly, Ward et al. found that persons with patella alta had larger quadriceps moment arms than control subjects [23]. Neither of these studies conducted a sensitivity analysis to assess the effects of various degrees of patella alta. In addition, our study was the first to analyze how varying tibial tubercle length affects quadriceps effective moment arm.

In addition, the findings of the Hinged TKR Model were partially consistent with the findings of Long et al. [32], who used an Oxford rig-style knee simulator to study design considerations in hinged TKR's. By evaluating five commercially available knee implants, they concluded that, while the anterior-posterior position of the hinge plays a role in determining patellar tendon moment arm, there are other factors at play such as the geometry of the patellofemoral joint. They found that a more posterior hinge produces a greater patellar tendon moment arm at 20 degrees knee flexion but noted that the opposite may be true at greater knee flexion angles. Likewise, they found that a more posterior hinge can reduce quadriceps force, which can reduce patellofemoral contact force. However, they did not comment directly on the relationship between hinge position and contact force. Consistent with our study, they also found that the greatest patellar tendon moment arm occurs at 20 degrees of knee flexion in hinged knee replacements. [32] studied commercially available implants in three dimensions, which likely revealed nuances that were neglected by our planar model. In addition, Browne et al. stated that a more posterior flexion axis tends to increase extensor moment arm in hinged knee replacements, which was consistent with our findings [36]. This was the first study that employed a sensitivity analysis to characterize the direct impact of hinge position on quadriceps moment arm and patellofemoral contact force.

Finally, the findings of the Hinged TKR Model with Knee Simulator Input agreed with the findings of Maletsky et al. [33], who used an Oxford-rig style knee simulator in conjunction with a planar model to study the tibiofemoral force in condylar TKR implants. Their results demonstrated that a planar equilibrium model can make realistic predictions of forces in the knee, and this study applied their methodology to accurately predict patellofemoral contact force, patella angle, and patellar ligament moment arm. The two studies differ in that [33] was focused on condylar implants and tibiofemoral force, while ours was focused on hinged implants that do not exhibit tibiofemoral contact force. This study both extended and complimented the work of [33] by extending their methodology to a different type of implant and predicting different measurements.

## 5.3 Implications

Based on the results of this study, we learned that planar equilibrium knee models can be a legitimate tool for studying natural and artificial human knees. When used as a research tool, our models proved robust enough to perform sensitivity analyses that simulated structural changes not found in the typical human knee. Specifically, the findings of the Osgood-Schlatter sensitivity study suggested that a condition developed in adolescence can result in structural changes that permanently change the quadriceps moment arm, and as a result, the efficiency of the knee. However, more research is required to confirm or deny this assertion. In addition, the Hinged TKR Model suggested that a posterior hinge can produce two major benefits: 1) Increased leverage and efficiency of the quadriceps and 2) Reduced patellofemoral contact force. Both of these benefits may significantly improve TKA outcomes, especially for elderly and disabled patients who more commonly receive hinged implants. Greater leverage in the quadriceps means elderly and disabled patients may be able to perform everyday activities despite weaker quadriceps muscles, while reduced patellofemoral contact force may reduce postoperative pain. However, given the complexity of TKA, human subjects trials would be necessary to validate these claims. Finally, the Hinged TKR Model with Knee Simulator Input upheld the fact that a computationally efficient planar equilibrium model can make predictions that are consistent with mechanical knee simulators. As a result, planar models may be able to predict additional measurements that were not considered in our study. In addition, a planar equilibrium model could prove useful in the design of TKR implants as a rapid prototyping tool. Without having to create separate CAD models or physical prototypes, a planar equilibrium model could evaluate hundreds of potential designs and predict measurements of moment arms, contact forces and more.

## 5.4 Limitations

Certain limitations affected this study, most of which arose from the assumptions used to construct the planar models. This study assumed that all forces and motions of knee extension occur in the sagittal plane, which neglected the three dimensional geometries of the human knee. For example, the patella was assumed to “roll” along a curve with a single point of contact. However, patellofemoral motion in the human knee occurs in three dimensions, and the patellofemoral contact force is transmitted over an area, rather than at a single point. Similarly, the quadriceps was assumed to attach to the patella at a single point and act along the long axis of the femur. However, in reality the quadriceps has a broad attachment to the patella through the patellar tendon and is made up of multiple smaller muscles that pull in different directions. This broad attachment produces dynamics during knee extension that were not accounted for in our models. Furthermore, the natural knee and TKR implants were both assumed to be frictionless. Although natural and artificial knees are well-lubricated, there is nonetheless friction present at every point of contact. This friction produces wear on the knee and adds complexity to the dynamics of knee extension. Finally, all of the components of the knee model were assumed to be rigid and inextensible, particularly the patellar ligament, which in reality stretches during knee extension. Despite these limitations, the planar equilibrium model demonstrated excellent agreement with the PSKS. Indeed, many assumptions were made for the sake of simplicity and computational efficiency; however, the results of this study suggest that the essence of knee extension can be captured by a planar equilibrium model.

### 5.5 General Conclusions and Future Studies

This study presented three planar equilibrium models of the human knee. The first, the Natural Knee Model, characterized the impact of Osgood-Schlatter on knee mechanics. The second, the Hinged TKR Model, shed light on the impact of the A-P position of the hinge, perhaps the most important design consideration in hinged knee implants. The third model, the Hinged TKR Model with Knee Simulator Input, used the planar knee model to augment the Penn State Knee Simulator. Ultimately, this study demonstrated the utility of planar equilibrium knee models and their ability to accurately predict measurements in both natural and artificial knees. In future studies, we would expand on this study in the following ways:

- Refine the model code and create a “tool” with a user interface that would empower researchers and implant engineers to use planar equilibrium models to study knee mechanics.
- Create a “virtual knee simulator” that uses a planar model to predict quadriceps force and feeds it into a second planar model.
- Recruit human subjects and tailor a model to each subject. Then, compare model outputs to experimental measurements and motion capture data.
- Modify the PSKS and/or planar model to simulate more dynamic activities like running, climbing stairs, and jumping.
- Study TKA outcomes in patients with hinged implants and characterize the impact of a posterior hinge. Compare these results to those predicted by the planar model.

# Appendix A

# MATLAB Code

## Natural Knee Model

### Natural Knee Sensitivity Analysis Driver

This script performs the sensitivity analysis described in 3.1.

```
clear
close all
clc

%% Define Inputs and Parameters
% Note: distances in cm, angles in deg, forces in Newtons
% Those parameters used later in the driver
% are stored as meaningful variables

params.TubLength = 0;  % INSTANTANEOUS advancement of tibial tuberosity
TibTubAdvancement = 1; % FINAL Advancement of Tibial Tuberosity
params.theta_q = 0;    % placeholder
% theta_q = theta defined in YZ_resid
params.tib_slope_angle = 8; %degrees
tib_slope_angle = params.tib_slope_angle;
params.Fq = 250;       % quad force
Fq = params.Fq;
params.TibAttachDist = 5.26;  % dist from tibial tuberosity
% to "top left corner" of tibia
TibAttachDist = params.TibAttachDist;
params.A1 = 3.54;      % femoral condyle (ellipse 1) axis lengths
params.B1 = 2.18;
params.A2 = 2.86;      % median anterior groove (ellipse 2) axis lengths
params.B2 = 1.90;
params.Lp = 3.94;      % length of patella
Lp = params.Lp;
params.t = 1.63;       % thickness of patella
params.Lpl = 6.52;     % length of patellar ligament
Lpl = params.Lpl;
NomRatio = Lpl/Lp;
params.L_tib_plat = 5.57; % length of tibial plateau
L_tib_plat = params.L_tib_plat;
params.Cx = .25;          % Cx, Cy =
Cx = params.Cx;           % location of the center of ellipse 2
params.Cy = .79;          % WRT ellipse 1 (in F)
Cy = params.Cy;

% Obtain location of TF contact point
% as percentage of tibial slope length
% *Data extracted from Fig 2 of Y+Z 1989 using 'Grabit' add-on*
load('Yamaguchi_fig_2_data.mat');
fig_2_x = Yamaguchi_fig_2_data(:,1);
fig_2_y = Yamaguchi_fig_2_data(:,2);
% perform spline fit or extracted fig 2 data
pct_tib_plat_vect = spline(fig_2_x, fig_2_y, 0:90)/100;

% Pre-allocate variables

x_soln = zeros(91,9);   % solution vector
residual = zeros(91,1); % total residual
```

```
resid2 = zeros(91,9);   % residual vector

% MA_1 is calculated geometrically (perp dist)
MA_act1 = zeros(91,1);
MA_eff1 = zeros(91,10,10);
% MA_2 is calculated analytically (dL/d(theta))
FqLength = zeros(91,1);
MA_act2 = zeros(91,1);
MA_eff2 = zeros(91,10,10);
counter = .0001;


%% SOLVER- For loop runs simulation multiple times
% Lpl and tuburcle lentgh are varied
% to mimic patella alta and OS, respectively.

% The solver, post-processing, and animation all happen inside for loops
% that vary Lpl and TubLength

% The solver itself, and many post-calculations, must be performed at every
% angle theta for the given trial, hence another for loop from 1 to 90 deg

Lpl_vect = linspace(6.5,7.2,10);

for i = 0:9
    % change tuburcle length (OS)
    params.TubLength = TibTubAdvancement*.1*i;
    TubLength = params.TubLength;
    for j = 0:9

        frac = counter/100;
        h_wait = waitbar(frac);
        waitbar(frac, h_wait, 'Running simulations... ')

        % changle Lpl (PA)
        Lpl = Lpl_vect(j+1);
        params.Lpl = Lpl;

        % specify initial guess, bounds
        %      Fr   Fpl  h  tx   ty  phi1 phi2  alpha beta
        x0 = [250  250  2  3    7.1 262  180   0    -30];
        lb = [0    0    0 -10  -15  200  100  -90   -90];
        ub = [500  500  Lp 10  15   400  300   90    90];


        for theta = 0:90

            ind = theta + 1;

            pct_tib_plat = pct_tib_plat_vect(ind);

            % f passes theta, params into YZ_resid
            f = @(x)YZ_resid(x,theta,pct_tib_plat,params);
            % call to solver, generate solution and residual vectors

            [x_soln(ind,:),residual(ind)] = lsqnonlin(f,x0,lb,ub);%opts);

            % guess at next theta is soln to previous theta
            x0 = x_soln(ind,:);
            resid2(ind,:) = YZ_resid(x_soln(ind,:),theta,pct_tib_plat,params);

            % extract necessary values from solution vector
            Fpl = x_soln(ind,2);
            tx = x_soln(ind, 4);
            ty = x_soln(ind, 5);
            alpha = x_soln(ind,8);
            beta = x_soln(ind,9);

            % calculate moment arm 1 (geometric)
            %{
```

```
 A O (Bottom left of patella)
    \
     \          C (TF Contact point)
      \   ______O_______
       \ |            /
        \|           /
      B  O          /
   (Tibial
  Tuberosity)

            %}

            % find theta2, angle between BA and BC
            BA = [-TubLength + Lpl*sind(beta)
                Lpl*cosd(beta)];
            BC = [TibAttachDist*sind(tib_slope_angle) + (1-
pct_tib_plat)*L_tib_plat*cosd(tib_slope_angle)
                TibAttachDist*cosd(tib_slope_angle) - (1-
pct_tib_plat)*L_tib_plat*sind(tib_slope_angle)];
            theta2 = acosd(dot(BA,BC)/(norm(BA)*norm(BC)));
            MA_act1(ind,:) = (dot(BA,BC)/norm(BA))*tand(theta2);

            % calculate EFFECTIVE moment arm 1
            MA_eff1(ind,i+1,j+1) = Fpl*MA_act1(ind,:)/Fq;



        end

        counter = counter + 1;

        %% Calculate weighted residual vector
        WeightedResid = resid2;
        WeightedResid(:,1:2) = .1*resid2(:,1:2)/Fq;
        [max_resid,index] = max(abs(WeightedResid), [], 'all', 'linear');

        if max_resid > 10^-3
            warning('Significant error detected.')
            fprintf('Error of %4.6f found at index %4.0f of WeightedResid. \n',max_resid, index)
            pause
        else
            fprintf('No significant error detected. \n')
        end

        % Animate?
        {
        choice = menu('Animate?', 'Yes', 'No');
        if choice == 1
            run YZ_anim_driver.m
        end
        }

    end
end
frac = 1;
```

## Natural Knee Residual Function

This function accepts the input parameters and current solution vector of the model and returns the residual vector.

```
function f = YZ_resid(x,theta,pct_tib_plat,params)

% Inputs and parameters
TubLength = params.TubLength;
```

```
params.theta_q = theta;
theta_q = params.theta_q;
tib_slope_angle = params.tib_slope_angle;
Fq = params.Fq;
TibAttachDist = params.TibAttachDist;
A1 = params.A1;
B1 = params.B1;
A2 = params.A2;
B2 = params.B2;
Lp = params.Lp;
t = params.t;
Lpl = params.Lpl;
L_tib_plat = params.L_tib_plat;
Cx = params.Cx;
Cy = params.Cy;

% Specify unknowns
Fr = x(1);     % patllafemoral contact force
Fpl = x(2);    % Patellar ligament force
h = x(3);      % dist from bottom of patella to PF contact point
tx = x(4);     % location of origin of F CS in T
ty = x(5);
phi1 = x(6);   % ellipse 1 parameter
phi2 = x(7);   % ellipse 2 parameter
alpha = x(8); % angle between patella and vertical
beta = x(9);   % angle between patellar ligament and vertical



% 9 EQUATIONS FORMING RESIDUAL VECTOR
f = zeros(1,9);

% Static Equilibrium:
f(1) = -cosd(alpha)*Fr - sind(beta)*Fpl + sind(theta_q)*Fq;
f(2) = sind(alpha)*Fr - cosd(beta)*Fpl + cosd(theta_q)*Fq;
temp = cross([-t -h 0], [Fpl*sind(alpha - beta) -Fpl*cosd(alpha - beta) 0])...
    + cross([-t Lp-h 0], [Fq*sind(theta_q - alpha) Fq*cosd(theta_q - alpha) 0]);
f(3) = temp(3);


% TF Contact Point:
Ttf = [ cosd(theta)  sind(theta)  0  tx;
       -sind(theta)  cosd(theta)  0  ty;
        0            0            1  0 ;
        0            0            0  1];
temp = Ttf*[A1*cosd(phi1); B1*sind(phi1); 0; 1];

f(4) = TibAttachDist*sind(tib_slope_angle) + (1-pct_tib_plat)*L_tib_plat*cosd(tib_slope_angle) -
temp(1);
f(5) = TibAttachDist*cosd(tib_slope_angle) - (1-pct_tib_plat)*L_tib_plat*sind(tib_slope_angle) -
temp(2);

vect1 = Ttf*[-A1*sind(phi1); B1*cosd(phi1); 0; 0];
vect1 = vect1/norm(vect1);
vect2 = [cosd(tib_slope_angle); -sind(tib_slope_angle); 0];
temp = cross(vect1(1:3), vect2);
f(6) = temp(3);


% PF Contact Point
temp = Ttf*[Cx + A2*cosd(phi2); Cy + B2*sind(phi2); 0; 1];
f(7) = -TubLength + Lpl*sind(beta) + t*cosd(alpha) + h*sind(alpha) - temp(1);
f(8) = Lpl*cosd(beta) - t*sind(alpha) + h*cosd(alpha) - temp(2);

vect1 = Ttf*[-A2*sind(phi2); B2*cosd(phi2); 0; 0];
vect1 = vect1/norm(vect1);
vect2 = [sind(alpha); cosd(alpha); 0];
temp = cross(vect1(1:3), vect2);
f(9) = temp(3);
end
```

# Hinged TKR Model

## Hinged TKR Sensitivity Analysis Driver

This script performs the sensitivity analysis described in 3.2.

```
clear
close all
clc

% Status: Using dummy data, runs both models
% Next: verify output using actual hip frc data

%% Parameter Input

% specify points that splines are based on
pat_spline_pts =  [ 0.2878328   -1.51866092;
    0.53875686  -1.16105178;
    0.69176138  -0.86296246;
    0.78161642  -0.60709048;
    0.84768944  -0.28579318;
    0.86614      0;
    0.83076796   0.3949446;
    0.74197972   0.7324471;
    0.63265812   0.99162362;
    0.4649216    1.27374904;
    0.2878328    1.51866092]';

fem_spline_pts = [ -1.31203954  -0.64701674;
    -1.81688232  -0.64701674;
    -2.30312468  -0.52940204;
    -2.8309316   -0.33295844;
    -3.2822388   -0.09787128;
    -3.6622736    0.178838098;
    -3.9760144    0.51293776;
    -4.1839134    0.86360254;
    -4.3224704    1.31477258;
    -4.356735     1.68402254;
    -4.349115     2.14546434;
    -4.3411902    2.5994868;
    -4.3331384    3.0612842;
    -4.3266614    3.43154;
    -4.3205146    3.7842698;
    -4.3147996    4.111371]';

% make parameter vectors that can be used for spline fitting
pat_param = 0:length(pat_spline_pts(1,:))-1;
fem_param = 0:length(fem_spline_pts(1,:))-1;

% fit splines
data.pat_pp = csapi(pat_param,pat_spline_pts);
data.fem_pp = csapi(fem_param,fem_spline_pts);

% find derivatives of splines
data.pat_der_pp = fnder(data.pat_pp,1);
data.fem_der_pp = fnder(data.fem_pp,1);

% point definitions
data.hinge_in_t = [3.44853 5.99815 0 1]';
data.Q_orig_in_f = [-4.09633 58.22908 0 1]';
data.Q_ins_in_p = [-0.36120 3.30501 0 1]';
data.PL_orig_in_p = [-0.40121 -3.03964 0 1]';
data.PL_ins_in_t = [0 0 0 1]';
data.PL_length = 6.93214;
```

```
nomx = 3.44853;
% decreased_x = linspace(nom_x - 0.5, nom_x, 6);
% increased_x = linspace(nom_x, nom_x + 0.5, 6);
hinge_x_vect = [nomx-0.75, nomx-0.5,nomx-0.25,nomx,nomx+0.25,nomx+0.50,nomx+0.75]';

%% General setup

opts_LSQ = optimoptions('lsqnonlin','Display','none','TolFun',1e-8,...
    'MaxIterations',100000);

nvars = 7;

% weight vector
%wt = [0.01 0.01   .5 6.0 6.0 50.0 6.0]'; % OG wt vector
wt = 100*[0.01 0.01 .05 6.0 6.0 50.0 6.0]';


theta_vec = 0:.2:90;
nsteps = length(theta_vec);

% DUMMY INPUTS
Fq = 1000;

%% Model #1 - initial setup/guess

tf_start1 = min(fem_param)+0.5*(max(fem_param)-min(fem_param));

% x = [Fr   Fpl    tp              tf          tx   ty   alpha  ]
x01 = [ 50   1000   mean(pat_param) tf_start1  -1.2  10   .1     ];
LB1 = [   0     0  min(pat_param)  min(fem_param)  -10   0   -30    ];
UB1 = [3000  3000  max(pat_param)  max(fem_param)   10  15   100   ];

MA_eff_vec1 = zeros(nsteps,1,length(hinge_x_vect));
all_x_opt1 = zeros(7,nsteps,length(hinge_x_vect));
all_resid1 = zeros(7,nsteps,length(hinge_x_vect));
all_resnorm = zeros(7,nsteps,length(hinge_x_vect));



%% Model #1 - vary theta and find positions

for i = 1:length(hinge_x_vect)

    data.hinge_in_t(1) = hinge_x_vect(i);

    x01 = [ 50   1000   mean(pat_param) tf_start1  -1.2  10   .1     ];

for ind = 1:nsteps

    theta = theta_vec(ind);

    [x_opt,rnorm,res,exitflag] = lsqnonlin(@(x) HingeResid_LSQ(x,theta,...
        Fq,data,wt),x01,LB1,UB1,opts_LSQ);
    all_resid1(:,ind,i) = res;

    x01 = x_opt;
    all_x_opt1(:,ind,i) = x_opt;
    all_resnorm(:,ind,i) = rnorm;

    fprintf('Percent completion: %4.2f %% exit = %i \n ', 100*ind/nsteps,exitflag)

    % calculate quad moment arm
    Fpl = x_opt(2);
    tx = x_opt(5);
    ty = x_opt(6);

    % "measure" MA_act, perp dist from hing to PL
    u_TF = [tx ty]'/norm([tx ty]);
    u_TH = data.hinge_in_t(1:2)'/norm(data.hinge_in_t(1:2));
    ang = acosd(dot(u_TF, u_TH));
```

```
    MA_act = norm(data.hinge_in_t(1:2))*sind(ang);

    % convert MA_act to eff quad MA
    MA_eff = Fpl*MA_act/Fq;
    MA_eff_vec1(ind,1,i) = MA_eff;

end

fprintf('Simulation is complete. \n')

figure(2),plot(all_resid1(:,:,i)','LineWidth',1.25)
figure(2),title('Residuals')
figure(2),legend('1','2','3','4','5','6','7')

figure(3),plot(all_x_opt1(1:7,:,i)','LineWidth',1.5)
figure(3),title('x soln (3-7)')
figure(3),legend('t_{p}','t_{f}','t_{x}','t_{y}','\alpha')


End
```

## Hinged TKR Residual Function

This function accepts the input parameters and current solution vector of the model and returns the residual vector.

```
function f = HingeResid_LSQ(x,theta,Fq,data,wt)

% x = [Fr Fpl tp tf tx ty alpha]
Fr = x(1);
Fpl = x(2);
tp = x(3);
tf = x(4);
tx = x(5);
ty = x(6);
alpha = x(7);

% define transformations: Fem-->Tib, Pat-->Tib
%   Pt = Ttf*Pf
%   Pt = Ttp*Pp
Ttf = [ cosd(theta) sind(theta) 0 data.hinge_in_t(1);
       -sind(theta) cosd(theta) 0 data.hinge_in_t(2);
        0          0            1 0;
        0          0            0 1            ];

Ttp = [ cosd(alpha) sind(alpha) 0 tx;
       -sind(alpha) cosd(alpha) 0 ty;
        0           0           1 0 ;
        0           0           0 1];


% attachment points - all 4x1
Q_orig_in_t = Ttf*data.Q_orig_in_f;
Q_ins_in_t = Ttp*data.Q_ins_in_p;
PL_orig_in_t = Ttp*data.PL_orig_in_p;
PL_ins_in_t = data.PL_ins_in_t;

% contact points - all 4x1
patCP_in_t = Ttp*[fnval(data.pat_pp,tp); 0; 1];
femCP_in_t = Ttf*[fnval(data.fem_pp,tf); 0; 1];

% patella force application points - all 4x1
r_Fq_in_t = Ttp*[data.Q_ins_in_p(1:3); 0];
r_Fpl_in_t = Ttp*[data.PL_orig_in_p(1:3); 0];
```

```
r_Fr_in_t = Ttp*[fnval(data.pat_pp,tp); 0; 0];

% spline derivatives - all 3x1
%   note that both splines must be defined as getting more superior as
%   tp and tf increase
pat_der_in_t = Ttp*[fnval(data.pat_der_pp,tp); 0; 0];
pat_der_in_t_u = pat_der_in_t(1:3)/norm(pat_der_in_t(1:3));
inward_pat_normal_in_t = [-pat_der_in_t_u(2); pat_der_in_t_u(1); 0];
fem_der_in_t = Ttf*[fnval(data.fem_der_pp,tf); 0; 0];
fem_der_in_t_u = fem_der_in_t(1:3)/norm(fem_der_in_t(1:3));

% forces on patella - all 3x1
Fq_in_t = Fq*(Q_orig_in_t(1:3) - Q_ins_in_t(1:3))/...
    norm(Q_orig_in_t(1:3) - Q_ins_in_t(1:3));
Fpl_in_t = Fpl*(PL_ins_in_t(1:3) - PL_orig_in_t(1:3))/...
    norm(PL_ins_in_t(1:3) - PL_orig_in_t(1:3));
Fr_in_t = Fr*inward_pat_normal_in_t;

% initialize unweighted residual vector
fu = zeros(7,1);

% static equilibrium of patella - forces
fu(1:2) = Fq_in_t(1:2) +  Fpl_in_t(1:2) + Fr_in_t(1:2);

% static equilibrium of patella - moments about pat orig
fu(3) = dot(cross(r_Fq_in_t(1:3),Fq_in_t),[0 0 1]) + ...
       dot(cross(r_Fpl_in_t(1:3),Fpl_in_t),[0 0 1]) + ...
       dot(cross(r_Fr_in_t(1:3),Fr_in_t),[0 0 1]);

% contact between femur and patella
fu(4:5) = femCP_in_t(1:2) - patCP_in_t(1:2);
fu(6) = dot(cross(fem_der_in_t_u,pat_der_in_t_u),[0 0 1]);

% constant length PL
fu(7) = norm(PL_orig_in_t(1:3)-PL_ins_in_t(1:3)) - data.PL_length;

% weighted residual vector
f = wt.*fu;

end
```

# Hinged TKR with Knee Simulator Input

## Hinged TKR with PSKS Input Driver

This script performs the analysis described in 3.3.

```
clear all
close all

% specify points that splines are based on
pat_spline_pts =  [ 0.2878328   -1.51866092;
    0.53875686  -1.16105178;
    0.69176138  -0.86296246;
    0.78161642  -0.60709048;
    0.84768944  -0.28579318;
    0.86614       0;
    0.83076796   0.3949446;
    0.74197972   0.7324471;
    0.63265812   0.99162362;
    0.4649216    1.27374904;
    0.2878328    1.51866092]';
```

```
fem_spline_pts = [ -1.31203954  -0.64701674;
    -1.81688232  -0.64701674;
    -2.30312468  -0.52940204;
    -2.8309316   -0.33295844;
    -3.2822388   -0.09787128;
    -3.6622736    0.178838098;
    -3.9760144    0.51293776;
    -4.1839134    0.86360254;
    -4.3224704    1.31477258;
    -4.356735     1.68402254;
    -4.349115     2.14546434;
    -4.3411902    2.5994868;
    -4.3331384    3.0612842;
    -4.3266614    3.43154;
    -4.3205146    3.7842698;
    -4.3147996    4.111371]';

% make parameter vectors that can be used for spline fitting
pat_param = 0:length(pat_spline_pts(1,:))-1;
fem_param = 0:length(fem_spline_pts(1,:))-1;

% fit splines
data.pat_pp = csapi(pat_param,pat_spline_pts);
data.fem_pp = csapi(fem_param,fem_spline_pts);

% find derivatives of splines
data.pat_der_pp = fnder(data.pat_pp,1);
data.fem_der_pp = fnder(data.fem_pp,1);

% point definitions 10/15 tests
data.hinge_in_t = [3.44853 5.99815 0 1]';
data.Q_orig_in_f = [-4.09633 58.22908 0 1]';
data.Q_ins_in_p = [-0.36120 3.30501 0 1]';
data.PL_orig_in_p = [-0.40121 -3.03964 0 1]';
data.PL_ins_in_t = [0 0 0 1]';
data.PL_length = 6.93214;

% VMs for Nominal
fn_start = 'Nominal';
data.hinge_in_t = [3.73210 5.65487 0 1]';
data.Q_orig_in_f = [-4.35656 58.06256 0 1]';
data.Q_ins_in_p = [-0.48164 3.44336 0 1]';
data.PL_orig_in_p = [-0.78044 -3.08527 0 1]';
data.PL_ins_in_t = [0 0 0 1]';
data.PL_length = 7.03092;

ntrials = 5;

%% vary theta and find positions
opts = optimoptions('lsqnonlin','Display','none','TolFun',1e-6,...
    'MaxIterations',1000);
%all_x_opt = [];

PF_RMS = zeros(ntrials,1);
pat_ang_RMS = zeros(ntrials,1);
PTMA_RMS = zeros(ntrials,1);

for tr = 1:ntrials

    % weight vector
    wt = [1.0 1.0 5.0 1.0 1.0 5.0 1.0]';

    % Create initial plot

    % transformation between tibia and femur
    theta = 0;
    Ttf = [ cosd(theta) sind(theta) 0 data.hinge_in_t(1);
        -sind(theta) cosd(theta) 0 data.hinge_in_t(2);
        0          0            1 0;
```

```
    0          0            0 1            ];

% transformation between tibia and patella
alpha = 0;
tx = -2;
ty =  5;
Ttp = [ cosd(alpha) sind(alpha) 0 tx;
    -sind(alpha) cosd(alpha) 0 ty;
    0           0           1 0 ;
    0           0           0 1];

% get transformed points for initial plotting
pat_pts = get_transformed_pts(Ttp,pat_param,data.pat_pp,100);
fem_pts = get_transformed_pts(Ttf,fem_param,data.fem_pp,100);

% initial plotting, get handles to plot objects
figure(1),pat_h = plot(pat_pts(1,:),pat_pts(2,:),'r-');
axis([-10 10 -5 15])
axis equal
hold on
figure(1),fem_h = plot(fem_pts(1,:),fem_pts(2,:),'b-');
figure(1),cp_p_h = plot(pat_pts(1,1),pat_pts(2,1),'ro');
figure(1),cp_f_h = plot(fem_pts(1,1),fem_pts(2,1),'bo');

Q_orig_in_t = Ttf*data.Q_orig_in_f;
Q_ins_in_t  = Ttp*data.Q_ins_in_p;
figure(1),Q_h = plot([Q_orig_in_t(1) Q_ins_in_t(1)], ...
    [Q_orig_in_t(2) Q_ins_in_t(2)],'k-');

PL_orig_in_t = Ttp*data.PL_orig_in_p;
PL_ins_in_t  = data.PL_ins_in_t;
figure(1),PL_h = plot([PL_orig_in_t(1) PL_ins_in_t(1)], ...
    [PL_orig_in_t(2) PL_ins_in_t(2)],'k-');

%% initial guess
% x = [Fr Fpl tp tf tx ty alpha]
tf_start = min(fem_param)+0.8*(max(fem_param)-min(fem_param));
x0 = [   0.0  200.0 mean(pat_param) tf_start        -2   8   0];

% x = [Fr Fpl tp tf tx ty alpha]
LB = [   0.0    0.0 min(pat_param)  min(fem_param)  -4   6   0];
UB = [1500.0 1500.0 max(pat_param)  max(fem_param)   3  14  70];

fn = [fn_start '_' num2str(tr) '_out.mat'];
load(fn);

% filtering
fs = 100;
fc = 5;
theta_vec = lowpass(theta_vec, fs, fc);
alpha_vec = lowpass(alpha_vec, fs, fc);
Fq_vec    = lowpass(Fq_vec, fs, fc);
PF_vec    = lowpass(PF_vec, fs, fc);
PTMA_vec  = lowpass(PTMA_vec, fs, fc);

% find frame at which 90 degrees knee flexion is reached
endframe = 0;
for qq = 1:length(theta_vec)
    if (theta_vec(qq) > 90)
        endframe = qq;
        break
    end
end

frms = 1:5:endframe;
theta_vec = theta_vec(frms);
Fq_vec = 0.865779*Fq_vec(frms); % corrected calibration
alpha_vec = alpha_vec(frms);
PF_vec = PF_vec(frms);
PTMA_vec = 0.1*PTMA_vec(frms); % convert mm to cm
```

```
    nsteps = length(theta_vec);

    all_resid = zeros(7,nsteps);
    all_resnorm = zeros(1,nsteps);
    all_x_opt = zeros(nsteps,7);
    all_trials_x_opt(:,:,tr) = zeros(nsteps,7);

    for ind = 1:1:nsteps

        ind

        theta = theta_vec(ind);
        Fq = Fq_vec(ind);
        [x_opt,rnorm,res,exitflag] = lsqnonlin(@(x)
HingeResid_LSQ(x,theta,Fq,data,wt),x0,LB,UB,opts);
        all_resid(:,ind) = res;
        all_resnorm(ind) = rnorm;
        x0 = x_opt;
        all_x_opt(ind,:) = x_opt;
    end

    all_trials_x_opt(:,:,tr) = all_x_opt;

    LW = 1.5;
    MS = 7;

    figure(3),h1 = line_fewer_markers(theta_vec,Fq_vec,10,...
        '^-g','Spacing','curve','MarkerSize',MS,'MarkerFaceColor','g',...
        'LineWidth',LW);
    figure(3),h2 = line_fewer_markers(theta_vec,all_x_opt(:,1),10,...
        'o-r','Spacing','curve','MarkerSize',MS,'MarkerFaceColor','r',...
        'LineWidth',LW);
    figure(3),h3 = line_fewer_markers(theta_vec,PF_vec,10,...
        's-b','Spacing','curve','MarkerSize',MS,'MarkerFaceColor','b',...
        'LineWidth',LW);
    figure(3),h4 = line_fewer_markers(theta_vec,all_x_opt(:,2),10,...
        'd-k','Spacing','curve','MarkerSize',MS,'MarkerFaceColor','k',...
        'LineWidth',LW);
    figure(3),xlabel('Knee Flexion Angle (\theta) [deg]','FontName','Times New Roman')
    figure(3),ylabel('Force [N]','FontName','Times New Roman')
    figure(3),title('PF Contact Force and PL Force','FontName','Times New Roman')
    figure(3),legend([h2 h3 h4],'F_{r} (model)','F_{r} (exp)',...
        'F_{pl} (model)','Location','NorthWest','FontName','Times New Roman')
    axis([20 100 0 800])
    set(gcf,'color','w');

    figure(4),h1 = line_fewer_markers(theta_vec,all_x_opt(:,7),10,...
        'o-r','Spacing','curve','MarkerSize',MS,'MarkerFaceColor','r',...
        'LineWidth',LW);
    figure(4),h2 = line_fewer_markers(theta_vec,alpha_vec,10,'s-b',...
        'Spacing','curve','MarkerSize',MS,'MarkerFaceColor','b',...
        'LineWidth',LW);
    figure(4),xlabel('Knee Flexion Angle [deg]','FontName','Times New Roman')
    figure(4),ylabel('Patellar Angle (\alpha) [deg]','FontName','Times New Roman')
    figure(4),title('Patellar Angle (\alpha)','FontName','Times New Roman')
    figure(4),legend([h1 h2],'Model','Experiment','Location','SouthEast','FontName','Times New
Roman')
    axis([20 100 0 60])
    set(gcf,'color','w');

    figure(6),plot(all_resid')
    figure(6),legend('1','2','3','4','5','6','7')

    figure(7),plot(all_resnorm)

    PF_RMS(tr)      = sqrt(mean((all_x_opt(:,1)-PF_vec).^2));
    pat_ang_RMS(tr) = sqrt(mean((all_x_opt(:,7)-alpha_vec).^2));

    all_PTMA = zeros(nsteps,1);
```

```
anim_played = 0;
while (anim_played == 0)
    figure(1),title('PAUSED: Any key to display results (CTRL-c to quit)')
    pause(2.0)
    figure(1),title('Displaying animation')

    % display results
    for ind = 1:1:nsteps

        % transformation between tibia and patella
        tx    = all_x_opt(ind,5);
        ty    = all_x_opt(ind,6);
        alpha = all_x_opt(ind,7);
        Ttp = [ cosd(alpha) sind(alpha) 0 tx;
            -sind(alpha) cosd(alpha) 0 ty;
            0           0           1 0;
            0           0           0 1];

        % transformation between tibia and femur
        theta = theta_vec(ind);
        Ttf = [ cosd(theta) sind(theta) 0 data.hinge_in_t(1);
            -sind(theta) cosd(theta) 0 data.hinge_in_t(2);
            0          0            1 0;
            0          0            0 1            ];

        % get transformed points
        pat_pts = get_transformed_pts(Ttp,pat_param,data.pat_pp,100);
        fem_pts = get_transformed_pts(Ttf,fem_param,data.fem_pp,100);

        % update femur curves
        set(pat_h,'XData',pat_pts(1,:),'YData',pat_pts(2,:));
        set(fem_h,'XData',fem_pts(1,:),'YData',fem_pts(2,:));

        % update contact points
        cp_p = Ttp * [fnval(data.pat_pp,all_x_opt(ind,3)); 0; 1];
        set(cp_p_h,'XData',cp_p(1),'YData',cp_p(2));
        cp_f = Ttf * [fnval(data.fem_pp,all_x_opt(ind,4)); 0; 1];
        set(cp_f_h,'XData',cp_f(1),'YData',cp_f(2));

        Q_orig_in_t = Ttf*data.Q_orig_in_f;
        Q_ins_in_t  = Ttp*data.Q_ins_in_p;
        xd = [Q_orig_in_t(1) Q_ins_in_t(1)];
        yd = [Q_orig_in_t(2) Q_ins_in_t(2)];
        set(Q_h,'XData',xd,'YData',yd);

        PL_orig_in_t = Ttp*data.PL_orig_in_p;
        PL_ins_in_t  = data.PL_ins_in_t;
        xd = [PL_orig_in_t(1) PL_ins_in_t(1)];
        yd = [PL_orig_in_t(2) PL_ins_in_t(2)];
        set(PL_h,'XData',xd,'YData',yd);

        % compute PTMA
        B = PL_orig_in_t(1:2);
        A = [0 0]';
        H = data.hinge_in_t(1:2);
        avec = H-A;
        uvec = (B-A)/norm(B-A);
        bvec = dot(avec,uvec)*uvec;
        cvec = avec - bvec;
        all_PTMA(ind) = norm(cvec)

        axis([-10 10 -5 15])

        pause(0.01)
    end
    anim_played = 1;
end

PTMA_RMS(tr) = sqrt(mean((all_PTMA-PTMA_vec).^2));
```

```
    figure(5),h1 = line_fewer_markers(theta_vec,all_PTMA,10,...
        'o-r','Spacing','curve','MarkerSize',MS,'MarkerFaceColor','r',...
        'LineWidth',LW);
    figure(5),h2 = line_fewer_markers(theta_vec,PTMA_vec,10,'s-b',...
        'Spacing','curve','MarkerSize',MS,'MarkerFaceColor','b',...
        'LineWidth',LW);
    figure(5),xlabel('Knee Flexion Angle (\theta) [deg]','FontName','Times New Roman')
    figure(5),ylabel('MA_{pl} [cm]','FontName','Times New Roman')
    figure(5),title('Patellar Ligament MA','FontName','Times New Roman')
    figure(5),legend([h1 h2],'Model','Experiment','Location','SouthEast')
    axis([20 100 0 6])
    set(gcf,'color','w');


    %pause
    close all
end
mn_RMS_PF = mean(PF_RMS)
sd_RMS_PF = std(PF_RMS)

mn_RMS_ang = mean(pat_ang_RMS)
sd_RMS_ang = std(pat_ang_RMS)

mn_RMS_PTMA = mean(PTMA_RMS)
sd_RMS_PTMA = std(PTMA_RMS)
```

### Hinged TKR with PSKS Input Residual Function

This function is the same as the Hinged TKR Residual Function.

**BIBLIOGRAPHY**


[1] S. N. Williams, M. L. Wolford, and A. Bercovitz, "Hospitalization for Total Knee Replacement Among Inpatients Aged 45 and Over: United States, 2000–2010," *US Dep. Heal. Hum. Serv. Data Br.*, no. 210, p. 8, 2015, [Online]. Available: http://www.cdc.gov/nchs/data/databriefs/db186.htm.

[2] A. J. Price *et al.*, "Knee replacement," *Lancet*, vol. 392, no. 10158, pp. 1672–1682, 2018, doi: 10.1016/S0140-6736(18)32344-4.

[3] J. A. Singh, S. Yu, L. Chen, and J. D. Cleveland, "Rates of total joint replacement in the United States: Future projections to 2020-2040 using the national inpatient sample," *J. Rheumatol.*, vol. 46, no. 9, pp. 1134–1140, 2019, doi: 10.3899/jrheum.170990.

[4] M. Kazemi, Y. Dabiri, and L. P. Li, "Recent advances in computational mechanics of the human knee joint," *Comput. Math. Methods Med.*, vol. 2013, 2013, doi: 10.1155/2013/718423.

[5] G. T. Yamaguchi and F. E. Zajac, "A planar model of the knee joint to characterize the knee extensor mechanism," *J. Biomech.*, vol. 22, no. 1, pp. 1–10, 1989, doi: 10.1016/0021-9290(89)90179-6.

[6] T. A. Blackburn and E. Craig, "Knee Anatomy: A brief review," *Phys. Ther.*, vol. 60, no. 12, pp. 1556–1560, 1980, doi: 10.1016/S1557-0843(10)80004-1.

[7] R. S. Laskin, "The posterior cruciate ligament in total knee replacement," *Knee*, vol. 2, no. 3, pp. 139–144, 1995, doi: 10.1016/0968-0160(95)00022-4.

[8] A. Deburge, J. H. Aubriot, and J. P. Genet, "Current status of a hinge prosthesis (GUEPAR)," *Clin. Orthop. Relat. Res.*, vol. No. 145, pp. 91–93, 1979, doi: 10.1097/00003086-197911000-00011.

[9] A. S. Ranawat and C. S. Ranawat, "The history of total knee arthroplasty," *Knee Jt. Surg. Tech. Strateg.*, vol. 9782287993, no. 26, pp. 699–707, 2012, doi: 10.1007/978-2-287-99353-4_63.

[10] M. Bahraminasab and A. Jahan, "Material selection for femoral component of total knee replacement using comprehensive VIKOR," *Mater. Des.*, vol. 32, no. 8–9, pp. 4471–4477, 2011, doi: 10.1016/j.matdes.2011.03.046.

[11] T. A. Enab and N. E. Bondok, "Material selection in the design of the tibia tray component of cemented artificial knee using finite element method," *Mater. Des.*, vol. 44, pp. 454–460, 2013, doi: 10.1016/j.matdes.2012.08.017.

[12] P. Baker *et al.*, "Mid-term survival following primary hinged total knee replacement is good irrespective of the indication for surgery," *Knee Surgery, Sport. Traumatol. Arthrosc.*, vol. 22, no. 3, pp. 599–608, 2014, doi: 10.1007/s00167-012-2305-y.

[13] T. Gehrke, D. Kendoff, and C. Haasper, "The role of hinges in primary total knee replacement," *Bone Jt. J.*, vol. 96B, no. 11, pp. 93–95, 2014, doi: 10.1302/0301-

620X.96B11.34143.

[14] L. C. L. Nguyen, M. S. Lehil, and K. J. Bozic, “Trends in Total Knee Arthroplasty Implant Utilization,” *J. Arthroplasty*, vol. 30, no. 5, pp. 739–742, 2015, doi: 10.1016/j.arth.2014.12.009.

[15] C. A. Kahlenberg, B. U. Nwachukwu, A. S. McLawhorn, M. B. Cross, C. N. Cornell, and D. E. Padgett, “Patient Satisfaction After Total Knee Replacement: A Systematic Review,” *HSS J.*, vol. 14, no. 2, pp. 192–201, 2018, doi: 10.1007/s11420-018-9614-8.

[16] H. M. Kremers *et al.*, “Prevalence of total hip and knee replacement in the United States,” *J. Bone Jt. Surg. - Am. Vol.*, vol. 97, no. 17, pp. 1386–1397, 2014, doi: 10.2106/JBJS.N.01141.

[17] J. T. Evans, R. W. Walker, J. P. Evans, A. W. Blom, A. Sayers, and M. R. Whitehouse, “How long does a knee replacement last? A systematic review and meta-analysis of case series and national registry reports with more than 15 years of follow-up,” *Lancet*, vol. 393, no. 10172, pp. 655–663, 2019, doi: 10.1016/s0140-6736(18)32531-5.

[18] P. S. Walker and S. Sathasivam, “Design forms of total knee replacement,” *Proc. Inst. Mech. Eng. Part H J. Eng. Med.*, vol. 214, no. 1, pp. 101–119, 2000, doi: 10.1243/0954411001535282.

[19] S. Fornalski, M. H. McGarry, C. N. H. Bui, W. C. Kim, and T. Q. Lee, “Biomechanical effects of joint line elevation in total knee arthroplasty,” *Clin. Biomech.*, vol. 27, no. 8, pp. 824–829, 2012, doi: 10.1016/j.clinbiomech.2012.05.009.

[20] C. König *et al.*, “Joint line elevation in revision TKA leads to increased patellofemoral contact forces,” *J. Orthop. Res.*, vol. 28, no. 1, pp. 1–5, 2010, doi: 10.1002/jor.20952.

[21] R. P. Grelsamer, “Patella baja after total knee arthroplasty: Is it really patella baja?,” *J. Arthroplasty*, vol. 17, no. 1, pp. 66–69, 2002, doi: 10.1054/arth.2002.28728.

[22] R. P. Grelsamer and S. Meadows, “The Modified Insall-Salvati Ratio for Assessment of Patellar Height,” *Clin Orthop Relat Res.file///C/Users/amann/OneDrive - Pennsylvania State Univ. Lit. al. 2002- Patella Baja After Total Knee Arthroplast. .pdf*, no. 282, pp. 170–176, 1992.

[23] S. R. Ward, M. R. Terk, and C. M. Powers, “Influence of patella alta on knee extensor mechanics,” *J. Biomech.*, vol. 38, no. 12, pp. 2415–2422, 2005, doi: 10.1016/j.jbiomech.2004.10.010.

[24] I. Yoshii, L. A. Whiteside, S. E. White, and M. T. Milliano, “Influence of prosthetic joint line position on knee kinematics and patellar position,” *J. Arthroplasty*, vol. 6, no. 2, pp. 169–177, 1991, doi: 10.1016/S0883-5403(11)80013-6.

[25] J. Wismans, F. Veldpaus, J. Janssen, A. Huson, and P. Struben, “A three-dimensional mathematical model of the knee-joint,” *J. Biomech.*, vol. 13, no. 8, pp. 677–685, Jan. 1980, doi: 10.1016/0021-9290(80)90354-1.

[26] L. Blankevoort, J. H. Kuiper, R. Huiskes, and H. J. Grootenboer, “Articular contact in a three-dimensional model of the knee,” *J. Biomech.*, vol. 24, no. 11, pp. 1019–1031, 1991, doi: 10.1016/0021-9290(91)90019-J.

[27] T. M. G. J. van Eijden, E. Kouwenhoven, J. Verburg, and W. A. Weijs, “A mathematical model of the patellofemoral joint,” *J. Biomech.*, vol. 19, no. 3, 1986, doi: 10.1016/0021-9290(86)90154-5.

[28] J. L. Hicks, T. K. Uchida, A. Seth, A. Rajagopal, and S. L. Delp, “Is My Model Good Enough? Best Practices for Verification and Validation of Musculoskeletal Models and Simulations of Movement,” *J. Biomech. Eng.*, vol. 137, no. 2, pp. 1–24, 2015, doi: 10.1115/1.4029304.

[29] H. B. Henninger, S. P. Reese, A. E. Anderson, and J. A. Weiss, “Validation of computational models in biomechanics,” *Proc. Inst. Mech. Eng. Part H J. Eng. Med.*, vol. 224, no. 7, pp. 801–812, 2010, doi: 10.1243/09544119JEIM649.

[30] K. M. Varadarajan, R. E. Harry, T. Johnson, and G. Li, “Can in vitro systems capture the characteristic differences between the flexion-extension kinematics of the healthy and TKA knee?,” *Med. Eng. Phys.*, vol. 31, no. 8, pp. 899–906, 2009, doi: 10.1016/j.medengphy.2009.06.005.

[31] A. B. Zavatsky, “A kinematic-freedom analysis of a flexed-knee-stance testing Rig,” *J. Biomech.*, vol. 30, no. 3, pp. 277–280, 1997, doi: 10.1016/S0021-9290(96)00142-X.

[32] R. Long, S. Gheduzzi, T. A. Bucher, A. D. Toms, and A. W. Miles, “A biomechanical evaluation of hinged total knee replacement prostheses,” *Proc. Inst. Mech. Eng. Part H J. Eng. Med.*, vol. 227, no. 8, pp. 875–883, 2013, doi: 10.1177/0954411913488506.

[33] L. P. Maletsky and B. M. Hillberry, “Simulating dynamic activities using a five-axis knee simulator,” *J. Biomech. Eng.*, vol. 127, no. 1, pp. 123–133, 2005, doi: 10.1115/1.1846070.

[34] R. Nisell, G. Németh, and H. Ohlsén, “Joint forces in extension of the knee: Analysis of a mechanical model,” *Acta Orthop.*, vol. 57, no. 1, pp. 41–46, 1986, doi: 10.3109/17453678608993213.

[35] D. W. Lee, M. J. Kim, W. J. Kim, J. K. Ha, and J. G. Kim, “Correlation between magnetic resonance imaging characteristics of the patellar tendon and clinical scores in osgood-schlatter disease,” *Knee Surg. Relat. Res.*, vol. 28, no. 1, pp. 62–67, 2016, doi: 10.5792/ksrr.2016.28.1.62.

[36] C. Browne, J. C. Hermida, A. Bergula, C. W. Colwell, and D. D. D’Lima, “Patellofemoral forces after total knee arthroplasty: Effect of extensor moment arm,” *Knee*, vol. 12, no. 2, pp. 81–88, 2005, doi: 10.1016/j.knee.2004.05.006.

**ACADEMIC VITA**

# Anthony Mannarino IV

anthony4@psu.edu | LinkedIn: www.linkedin.com/in/ARMannarino

---

## Education

**The Pennsylvania State University | Schreyer Honors College | Anticipated Graduation: May 2022**
*College of Engineering* | B.S. Mechanical Engineering
*College of Liberal Arts* | B.S. Applied Spanish
***William and Wyllis Leonhard Engineering Scholar:*** A merit-based program offered to a select group of College of Engineering Students with exceptionally high ability and motivation.

---

## Related Work Experience

**Penn State Biomechanics Laboratory**
*September 2019 - present*
*Undergraduate Research Assistant*

- Collaborating with engineers from a major global medical device company to evaluate knee implant prototypes in the Penn State Knee Simulator
- Developing a simulation tool in MATLAB that will allow knee implant engineers to test their preliminary designs without having to build physical prototypes. This work is the basis of my Undergraduate Honors Thesis.
- Worked on an interdisciplinary team of five to streamline a 3D ultrasound technique to measure calf muscle volume in human subjects

***Languages:*** Fluency in Spanish, MATLAB, Arduino
***Skills:*** SolidWorks, Autodesk Fusion 360, Machine Learning, Circuit design, Mechanical Design, Microsoft Office

---

## Leadership and Involvement

**Penn State Dance Marathon (THON)**
*September 2019 - present*
*Training and Development Captain, Dancer Relations Committee*

- Leading a team of 75 volunteers to help plan and execute THON Weekend
- Training over 700 volunteers to ensure a safe and memorable experience during the 46-hour dance marathon
- Developing innovative fundraising techniques to raise money for the fight against childhood Cancer

**Penn State Marching Blue Band**
*August 2018 - present*
*Trombone Section Leader*

- Leading a team of 35 musicians—mentoring younger members, teaching marching fundamentals, and rehearsing up to 15 hours every week
- Maintaining perfect attendance at all rehearsals and performances, including the Citrus Bowl and Cotton Bowl